
Quantized Training of Gradient Boosting Decision Trees

Yu Shi^{1*} Guolin Ke^{2*†},
Zhuoming Chen^{3‡} Shuxin Zheng¹ Tie-Yan Liu¹
¹Microsoft Research ²DP Technology ³Tsinghua University
yushi2@microsoft.com, kegl@dp.tech
chen-zm19@mails.tsinghua.edu.cn, {shuxin.zheng, tyliu}@microsoft.com

Abstract

Recent years have witnessed significant success in Gradient Boosting Decision Trees (GBDT) for a wide range of machine learning applications. Generally, a consensus about GBDT’s training algorithms is gradients and statistics are computed based on high-precision floating points. In this paper, we investigate an essentially important question which has been largely ignored by the previous literature - *how many bits are needed for representing gradients in training GBDT?* To solve this mystery, we propose to quantize all the high-precision gradients in a very simple yet effective way in the GBDT’s training algorithm. Surprisingly, both our theoretical analysis and empirical studies show that the necessary precisions of gradients without hurting any performance can be quite low, e.g., 2 or 3 bits. With low-precision gradients, most arithmetic operations in GBDT training can be replaced by integer operations of 8, 16, or 32 bits. Promisingly, these findings may pave the way for much more efficient training of GBDT from several aspects: (1) speeding up the computation of gradient statistics in histograms; (2) compressing the communication cost of high-precision statistical information during distributed training; (3) the inspiration of utilization and development of hardware architectures which well support low-precision computation for GBDT training. Benchmarked on CPUs, GPUs, and distributed clusters, we observe up to $2\times$ speedup of our simple quantization strategy compared with SOTA GBDT systems on extensive datasets, demonstrating the effectiveness and potential of the low-precision training of GBDT. The code will be released to the official repository of LightGBM.⁴

1 Introduction

Gradient Boosting Decision Trees (GBDT) is a powerful machine learning algorithm. Despite the success of deep learning in recent years, GBDT is one of the best off-the-shelf choices of machine learning algorithms in many real-world tasks, including online advertising [33], search ranking [26, 14], finance prediction [29], etc. Along with carefully designed tools, including XGBoost [5], LightGBM [17], and CatBoost [24], GBDT has shown outstanding performance in various data science competitions [36] and industrial applications [32, 9, 28, 23].

Despite the success of GBDT, we found there is room for GBDT algorithms to fully exploit modern computation resources. First, the training of GBDT requires arithmetic operations of high-precision FP (Floating Point) numbers, which hinders the usage of low-precision computation resources. Low-precision training has become a standard technique to significantly accelerate the training of

*Corresponding authors.

†Work primarily done at Microsoft Research.

‡Work done during internship at Microsoft Research.

⁴<https://github.com/Microsoft/LightGBM>

neural networks [20]. The design of new processors for machine learning tends to encourage high throughput for low-precision computation. This results in a gap between GBDT training algorithms and the hardware architectures. Second, distributed training of GBDT is required for large datasets. The communication cost for distributed training, however, is huge due to high-precision statistical information passing among machines. The cost is especially high with a large number of features in the dataset, which hurts the scalability of GBDT in distributed systems.

In this paper, we propose a low-precision training algorithm for GBDT, based on stochastic gradient quantization. The main computation cost of training GBDT is the arithmetic operations over gradients. Before training each decision tree, we quantize the gradients into very low-precision (e.g., 2-bit or 3-bit) integers. Thus, we replace most of the FP arithmetic operations with integer arithmetic operations, which reduces computation time. In addition, low-bitwidth gradients result in a smaller memory footprint and better cache utilization. Techniques are proposed to preserve the accuracy of the model, including stochastic rounding in gradient quantization, and leaf-value refitting with original gradient values. We show both empirically and theoretically that quantized training of GBDT with low-bitwidth gradients is almost lossless in terms of model accuracy. Thus, we empower GBDT to utilize low-precision computation resources.

Distributed training of GBDT relies on the synchronization of gradient statistics. The gradient statistics are summarized into a histogram for each feature. With quantized gradients, only integer histogram values are needed in our algorithm. The communication among hosts or GPUs becomes sending and reducing of these integer values. And the size of these histograms is at least half of the original histograms with FP values. So quantized training of GBDT has an advantage in communication cost by nature and improves the scalability of GBDT on distributed systems.

We implement our system on both CPUs and GPUs. The results show that our methods accelerate the training of GBDT in various settings, including a single process on CPUs, a single process on a GPU, and distributed training over CPUs. This validates that our algorithm is general for different types of computation resources. Besides acceleration on existing hardware architectures, our algorithm also lay the foundation for GBDT to exploit new hardware architectures with more flexible support for low-precision operations in the future. Based on LightGBM, we implement a quantized GBDT training system. With quantized training, we achieve up to $2\times$ speedup compared with SOTA GBDT tools. Experiments also show that quantized GBDT training scales better in distributed systems.

Our algorithm also verifies huge redundancy in the information contained by gradient values in GBDT. Moreover, we reveal both theoretically and empirically how such redundancy can be properly reduced, to keep good model performance and training efficiency. And we show how to implement the quantized training of GBDT efficiently across different computation resources. We believe that these interesting findings will inspire new understandings and improvements for GBDT in the future.

2 Related Work

Trials to use low-precision training in deep neural networks (NN) are abundant. Using low bitwidth numbers in NN training can reduce memory access and accelerate training [13, 15, 35, 20, 10]. In addition to efficiency, the effectiveness of quantized NN training has also been discussed [7, 18, 4]. Besides quantization during the forward and backward calculations, quantization of gradients has also been applied in distributed training of neural networks [30] to reduce communication cost. However, the possibility of low-precision training for GBDT is rarely discussed in existing literature. RatBoost [22] is a boosting algorithm based on re-weighting samples. In RatBoost [22], quantization is applied to the weights of training samples during boosting, while the application of quantization in GBDT is not discussed. Recently gradient quantization is applied in federated training of GBDT [6] to transform FP gradients into large integers (e.g., 53-bit integers) for the sake of encryption. But quantization towards a very small number of bits is not explored. Accelerating GBDT training with quantized gradients was exploited by BitBoost [8]. And BitBoost shows empirically that it is possible to achieve comparable accuracy with quantized gradients of low bitwidth. However, BitBoost quantizes gradients in a deterministic way. In this paper, we provide a theoretical guarantee of quantized training based on stochastic quantization. And we show that stochastic quantization is crucial to preserve good model accuracy. Besides, BitBoost focuses on accelerating GBDT with bit operations on a single CPU core, and the implementation is a single-thread version. In this paper, we discuss important techniques in system implementation that enable significant acceleration across different computation platforms, including multi-core CPUs, GPUs, and distributed clusters.

Distributed training of GBDT is necessary for large-scale datasets. Training data are partitioned either by rows (data samples) or by columns (features) across different machines. We call the former strategy data-distributed training and the latter feature-distributed training. The communication cost for feature-distributed training grows linearly with the number of training samples [1, 19]. On the other hand, the communication cost for data-distributed training is proportional to the number of features [1, 19]. The two strategies can be combined with each machine getting only part of the features and samples [11]. The communication complexity of these strategies is analyzed in detail [31], with empirical studies [11]. Since training of GBDT requires summarizing the gradient statistics across the dataset into a histogram for each feature, the cost for data-distributed training is reduced with the more concise histogram information [5]. Thus, data-distributed training is more favorable with large-scale datasets. With many features, feature-distributed or the combination of two strategies can be faster [11].

Based on these distributed training strategies, some efforts have been made to reduce the communication cost. Meng et al [19] proposed Parallel-Voting Tree (PV-Tree) to further reduce the cost of data-distributed training. However, PV-Tree guarantees good performance only when different parts of the partitioned dataset have similar statistical distributions, which can require expensive random shuffling over the whole large dataset. Moreover, quantized training can be applied along with PV-Tree. This is because PV-Tree reduces communication cost by reducing the number of features to synchronize the statistics in the histograms. Since quantized training can reduce the size of histograms, it brings a general benefit for both PV-Tree and ordinary data-distributed training. DimBoost [16] keeps the number of communicated histograms unchanged but reduces the size of each histogram by compressing the histograms instead. Histograms represented by floating-point numbers in DimBoost are compressed into low-precision values (8-bit integers) before sending, and decoding into high-precision values. Note that in DimBoost, only the communication message for distributed training is in low-precision and the compression is lossy. In addition, reduction of the histograms still requires floating-point additions. In comparison, we quantized most parts of the training process of GBDT with low-precision integers, and only need to maintain histograms with integer values.

In this paper, we compare our algorithm with SOTA efficient implementations of GBDT, including XGBoost [5], LightGBM [17], and CatBoost [24]. They support training on CPUs, GPUs [34], and distributed training. However, none of these support low-precision training. We show that with quantized gradients, GBDT can be trained much faster compared with these SOTA tools in both single process and distributed settings, on both CPUs and GPUs. We implement quantized training based on LightGBM. But our method is general and can be adopted by all these tools.

3 Preliminaries of GBDT Algorithms

Gradient Boosting Decision Trees (GBDT) is an ensemble learning algorithm that trains decision trees as base components iteratively. In each iteration, for each training sample, the gradient (first-order derivative) and hessian (second-order derivative) of the loss function w.r.t. the current prediction value is calculated. Then a decision tree is trained to fit the negatives of gradients. Formally, in iteration $k + 1$, let \hat{y}_i^k be the current prediction value of sample i . And g_i and h_i are the gradient and hessian of loss function l :

$$g_i = \frac{\partial l(\hat{y}_i^k, y_i)}{\partial \hat{y}_i^k}, h_i = \frac{\partial^2 l(\hat{y}_i^k, y_i)}{(\partial \hat{y}_i^k)^2} \quad (1)$$

For a leaf s , denote I_s as the set of data indices in the leaf. Let $G_s = \sum_{i \in I_s} g_i$ and $H_s = \sum_{i \in I_s} h_i$ be the summations of g_i 's and h_i 's over samples in leaf s . With the tree structure being fixed in iteration $k + 1$, the training loss can be approximated by second-order Taylor polynomial:

$$\mathcal{L}_{k+1} \approx \mathcal{C} + \sum_s \left(\frac{1}{2} H_s w_s^2 + G_s w_s \right) \quad (2)$$

where \mathcal{C} is a constant and w_s is the prediction value of leaf s . By minimizing the approximated loss, we obtain the optimal value for leaf s and the minimal loss contributed by data in I_s :

$$w_s^* = -\frac{G_s}{H_s}, \quad \mathcal{L}_s^* = -\frac{1}{2} \cdot \frac{G_s^2}{H_s}. \quad (3)$$

Finding the optimal tree structure is difficult. Thus the tree is trained by greedily and iteratively splitting a leaf into two child leaves, starting from a single root leaf. When splitting leaf s into two

children s_1 and s_2 in tree T_{k+1} , we can calculate the reduction in the approximated loss

$$\Delta \mathcal{L}_{s \rightarrow s_1, s_2} = \mathcal{L}_s^* - \mathcal{L}_{s_1}^* - \mathcal{L}_{s_2}^* = \frac{G_{s_1}^2}{2H_{s_1}} + \frac{G_{s_2}^2}{2H_{s_2}} - \frac{G_s^2}{2H_s}. \quad (4)$$

To find the best split condition for leaf s , all split candidates of all features should be enumerated and the one with the largest loss reduction is chosen.

To accelerate the best split-finding process, an algorithm based on histograms is used by most state-of-the-art GBDT toolkits. The basic idea of histogram based GBDT is to divide the values of a feature into bins. Each bin corresponds to a range of feature values. Then we construct histograms with the bins such that each bin records the summation of gradients and Hessians of data in that bin. Only the boundaries of the bins (ranges) will be considered as candidates of split thresholds. Algorithm 1 describes the process of histogram construction. Bin data matrix `data` records for each feature and sample the index of the bin in the histogram, i.e., which range the feature value falls in. The g_i 's and h_i 's are accumulated in the corresponding bins in histograms of the features. Since the split

Algorithm 1 Histogram Construction for Leaf s

Input: Gradients $\{g_1, \dots, g_N\}$, Hessians $\{h_1, \dots, h_N\}$
Input: Bin data `data` $[N][J]$, Data indices in leaf s denoted by I_s
Output: Histogram `hist` $_s$
for $i \in I_s, j \in \{1 \dots J\}$ **do**
 $bin \leftarrow \text{data}[i][j]$
 `hist` $_s[j][bin].g \leftarrow \text{hist}_s[j][bin].g + g_i$
 `hist` $_s[j][bin].h \leftarrow \text{hist}_s[j][bin].h + h_i$
end for

criterion (4) only depends on the summation of gradient statistics, we can easily obtain the optimal split threshold by iterating over bins in the histogram. Traditionally 32-bit floating point numbers are used for g_i 's and h_i 's. And the accumulations in the histograms usually require 32-bit or 64-bit FP numbers. In the next section, we show how to quantizes g_i 's and h_i 's into low-bitwidth integers so that most of the arithmetic operations can be replaced with integer operations with a fewer number of bits, which substantially saves computational cost.

4 Quantized Training of GBDT

We describe our quantized training algorithm for GBDT. First, we show the overall framework. Then we identify the two critical techniques to preserve the accuracy of quantized training, including stochastic gradient quantization and leaf-value refitting.

4.1 Framework for Quantized Training

We first quantize g_i and h_i into low-bitwidth integers \tilde{g}_i and \tilde{h}_i . We divide the ranges of g_i 's and h_i 's of all training samples into intervals of equal length. To use B -bit ($B \geq 2$) integer gradients, we use $2^B - 2$ intervals. Each end of the intervals corresponds to an integer value, resulting in $2^B - 1$ integer values in total. Since the first-order derivatives g_i 's can take both positive and negative values, half of the intervals will be allocated for the negative values, and the other half for the positive values. For the second-order derivatives h_i 's, almost all commonly used loss functions of GBDT have non-negative values. We assume that $h_i \geq 0$ in subsequent discussions. Thus the interval lengths are

$$\delta_g = \frac{\max_{i \in [N]} |g_i|}{2^{B-1} - 1}, \quad \delta_h = \frac{\max_{i \in [N]} h_i}{2^B - 2} \quad (5)$$

for g_i 's and h_i 's, respectively. Then we can calculate the low-bitwidth gradients

$$\tilde{g}_i = \text{Round} \left(\frac{g_i}{\delta_g} \right), \quad \tilde{h}_i = \text{Round} \left(\frac{h_i}{\delta_h} \right). \quad (6)$$

The function *Round* rounds a floating point number into an integer number. Note that in the case where h_i 's are constant, there's no need to quantize h_i . We left the detailed rounding strategy in Section 4.2. We replace g_i 's and h_i 's in Algorithm 1 with \tilde{g}_i 's and \tilde{h}_i 's. Then addition operations of the original gradients can be directly replaced by integer additions. Concretely, the statistics g and h in the histogram bins will become integers. Thus accumulating gradients into histogram bins in

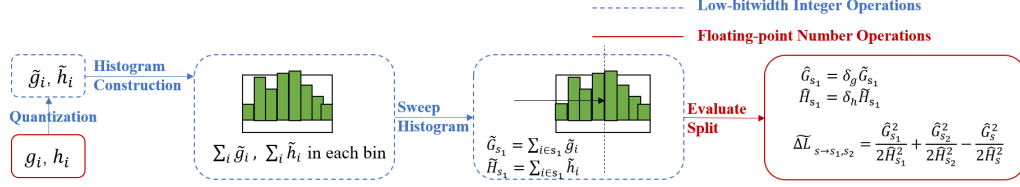


Figure 1: Workflow of the quantized GBDT training.

Algorithm 1 only requires integer additions. In equation (4), G_{s_1} , H_{s_1} , G_{s_2} and H_{s_2} will be replaced by their integer counterparts \tilde{G}_{s_1} , \tilde{H}_{s_1} , \tilde{G}_{s_2} , and \tilde{H}_{s_2} . We found that 2 to 4 bits for quantized gradients are enough for good accuracy. As we will discuss in Section 6.1 and 7.4.3, in most cases, 16-bit integers will be enough to accumulate such low-bitwidth gradients in histograms. Thus, most of the operations are done with low-bitwidth integers. We only need floating point operations when calculating the original gradients, Hessians and the split gain. Specifically, the split gain is estimated as

$$\Delta \tilde{\mathcal{L}}_{s \rightarrow s_1, s_2} = \frac{(\tilde{G}_{s_1} \delta_g)^2}{2\tilde{H}_{s_1} \delta_h} + \frac{(\tilde{G}_{s_2} \delta_g)^2}{2\tilde{H}_{s_2} \delta_h} - \frac{(\tilde{G}_s \delta_g)^2}{2\tilde{H}_s \delta_h}, \quad (7)$$

where the scale of the gradient statistics is recovered by multiplying δ_g and δ_h . Figure 1 summarizes the workflow for quantized GBDT training.

4.2 Rounding Strategies and Leaf-Value Refitting

We find that the *Round* strategy in equation (6) has a significant impact on the accuracy of the quantized training algorithm. Rounding to the nearest integer number seems to be a reasonable choice. However, we found the accuracy drops severely with this strategy, especially with a small number of gradient bits. Instead, we adopt a stochastic rounding strategy. \tilde{g}_i randomly takes values $\lfloor g_i/\delta_g \rfloor$ or $\lceil g_i/\delta_g \rceil$ such that $\mathbb{E}[\tilde{g}_i] = g_i/\delta_g$. The formal definitions of the two rounding strategies are

$$\text{RN}(x) = \begin{cases} \lfloor x \rfloor, & x < \lfloor x \rfloor + \frac{1}{2} \\ \lceil x \rceil, & x \geq \lfloor x \rfloor + \frac{1}{2} \end{cases}, \quad \text{SR}(x) = \begin{cases} \lfloor x \rfloor, & \text{w.p. } \lfloor x \rfloor - x \\ \lceil x \rceil, & \text{w.p. } x - \lfloor x \rfloor \end{cases} \quad (8)$$

where we use RN for round-to-nearest and SR for stochastic rounding. The key insight is that the split gain is calculated with the summation of gradients. And stochastic rounding would provide an unbiased estimation for the summations, i.e. $\mathbb{E}[\tilde{G} \delta_g] = G$, and $\mathbb{E}[\tilde{H} \delta_h] = H$ in equation (7). The importance of stochastic rounding is also recognized in other scenarios for quantization, including NN quantization training [13] and histogram compression in DimBoost [16]. With stochastic rounding, we provide a theorem in Section 5 which ensures that the error in split gain estimation caused by quantized gradients is bounded by a small value with high probability.

With quantized gradients, the optimal leaf value in equation (3) becomes $\tilde{w}_s^* = -\frac{\tilde{G}_s \delta_g}{\tilde{H}_s \delta_h}$. In most cases, \tilde{w}_s^* is enough for good results. But we found that for some loss functions, especially ranking objectives, refitting the leaf values with the original gradients after the tree has stopped growing is useful to improve the accuracy of quantized training. BitBoost [8] also recalculates leaf values with real gradients after tree growing. The difference is that here we consider Hessians in split gain (7) during tree growth, but BitBoost treats Hessians as constants during tree growth and uses true Hessians only when refitting the leaf values. It is cheap to calculate w_s^* in equation (3) given a fixed tree structure since only a single pass over g_i 's and h_i 's is needed to sum them up into different leaves.

5 Theoretical Analysis

We prove that the difference in the gain of a split due to gradient quantization is bounded by a small value, with enough training data. We consider loss functions with constant second-order derivatives (i.e., the h_i 's are constant). The square error loss function $l(\hat{y}, y) = \frac{1}{2}(\hat{y} - y)^2$ for regression tasks falls in this category. The analysis is also fit for GBDT without second-order Taylor approximation. We leave the case for loss functions with non-constant second-order derivatives in Appendix B. We focus on the discussion of the conclusion in this section and leave details of the proof in Appendix B.

Our theoretical analysis is based on a more specific form of weak-learnability assumption in boosting. Specifically, the assumption considers only two-leaf decision trees (a.k.a. stumps) as weak learners.

Definition 5.1 (Weak Learnability of Stumps) Given a binary classification dataset $\mathcal{D} = \{(\mathbf{x}_i, c(\mathbf{x}_i))\}_{i=1}^N$ where $c(\mathbf{x}_i) \in \{-1, 1\}$, weights $\{w_i\}_{i=1}^N$, $w_i \geq 0$ and $\sum_i w_i > 0$, there exists $\gamma > 0$ and a two-leaf decision tree with leaf values in $\{-1, 1\}$ s.t. the weighted classification error rate on \mathcal{D} is $\frac{1}{2} - \gamma$. Then the dataset \mathcal{D} is γ -empirically weakly learnable by stumps w.r.t. c and $\{w_i\}_{i=1}^N$.

The weak learnability of stump states that given a binary-class concept c and weights for dataset \mathcal{D} , there exists a stump that can produce slightly better classification accuracy than a random guess. Our analysis is based on the following assumption over the data in a single leaf s .

Assumption 5.2 Let $\text{sign}(\cdot)$ be the sign function (with $\text{sign}(0) = 1$). For data subset $\mathcal{D}_s \subset \mathcal{D}$ in leaf s , there exists a stump and a $\gamma_s > 0$ s.t. \mathcal{D}_s is γ_s -empirically weakly learnable by stumps, w.r.t. concept $c(\mathbf{x}_i) = \text{sign}(g_i)$ and weights $w_i = |g_i|$, where $i \in I_s$.

An equivalence of the assumption is: \mathcal{D} is γ_s -empirically weakly learnable by stumps, w.r.t. concept $c(\mathbf{x}_i) = \text{sign}(g_i)$, and weights $w_i = |g_i|$ for $i \in I_s$ and $w_i = 0$ for $i \in [N] \setminus I_s$. A similar assumption has been adopted in previous theoretical analysis for gradient boosting [12]. The difference is that here we restrict the weak learner to be a stump. In Appendix B, we show that for any leaf s with positive split gain, there exists such a $\gamma_s > 0$. As we will see in the experiments, for most leaves during the training of GBDT, γ_s won't be too small.

Let $\mathcal{G}_{s \rightarrow s_1, s_2} = -(\mathcal{L}_{s_1}^* + \mathcal{L}_{s_2}^*) \geq 0$, where $\mathcal{L}_{s_1}^*$ and $\mathcal{L}_{s_2}^*$ are defined in equation (3). And let $\tilde{\mathcal{G}}_{s \rightarrow s_1, s_2} = -(\tilde{\mathcal{L}}_{s_1}^* + \tilde{\mathcal{L}}_{s_2}^*) \geq 0$ be the estimated version of $\mathcal{G}_{s \rightarrow s_1, s_2}$ after gradient quantization. And let $\mathcal{G}_s^* = \mathcal{G}_{s \rightarrow s_1^*, s_2^*}$ be the value for the optimal split $s \rightarrow s_1^*, s_2^*$ in leaf s . Note that for leaf s , the optimal split is chosen only according to $\mathcal{G}_{s \rightarrow s_1, s_2}$, since \mathcal{L}_s^* is a constant for different splits of leaf s . Then based on Assumption 5.2, we have the following theorem.

Theorem 5.3 For loss functions with constant hessian value $h > 0$, if Assumption 5.2 holds for the subset \mathcal{D}_s in leaf s for some $\gamma_s > 0$, then with stochastic rounding and leaf-value refitting, for any $\epsilon > 0$, and $\delta > 0$, at least one of the following conclusions holds:

1. With any split of leaf s and its descendants, the resultant average of absolute values of prediction values by the tree in the current boosting iteration for data in \mathcal{D}_s is no greater than ϵ/h .
2. For any split $s \rightarrow s_1, s_2$ of leaf s , with a probability of at least $1 - \delta$,

$$\frac{|\tilde{\mathcal{G}}_{s \rightarrow s_1, s_2} - \mathcal{G}_{s \rightarrow s_1, s_2}|}{\mathcal{G}_s^*} \leq \frac{\max_{i \in [N]} |g_i| \sqrt{2 \ln \frac{4}{\delta}}}{\gamma_s^2 \epsilon \cdot 2^{B-1}} \left(\sqrt{\frac{1}{n_{s_1}}} + \sqrt{\frac{1}{n_{s_2}}} \right) + \frac{\left(\max_{i \in [N]} |g_i| \right)^2 \ln \frac{4}{\delta}}{\gamma_s^2 \epsilon^2 n_s \cdot 4^{B-2}}. \quad (9)$$

In equation (9), the bound of gradients $\max_{i \in [N]} |g_i|$ is determined by the labels and the loss function. For regression tasks, we can normalize the labels to a fixed range, e.g., $[0, 1]$, thus the gradients are bounded. For classification tasks, the gradients are bounded (in the range $[-1, 1]$) by nature with cross-entropy loss. With enough data in leaf s , if the split is not too imbalanced and partitions enough data into both children s_1 and s_2 , then we can expect the error caused by quantization is small. Theorem 5.3 ensures that with quantized training, either a split of a leaf has a limited impact on the prediction values, or quantization does not change the gains of the splits too much.

In equation (9), we also notice that with more bits (larger B) to represent gradients in quantization, the error will be smaller. This is consistent with our intuition that with more quantized values, we can approximate the original gradients better. But in practice, we found that a smaller number of bits (e.g., 2 to 4 bits) is enough for good accuracy. With $n_s = 10^7$ in parent node s , and $n_{s_1} = n_{s_2} = 5 \times 10^6$. Let $\epsilon = \max_{i \in [N]} |g_i| / 10$, assume that in leaf s we have $\gamma_s = 0.2$ and let $\delta = 0.1$. With 3 bits for gradients, the upper bound in (9) is approximately 0.15. With 4 bits, the value is smaller than 0.08. Thus, with a high probability (greater than 90%), changes in split gain due to quantization is well bounded.

We have a similar analysis for the cases where Hessians h_i 's are not constant. For non-constant hessian values, the analysis requires additional assumptions. Due to limited space, we left the details in Appendix B.

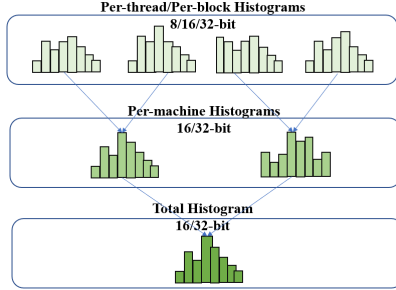


Figure 2: Hierarchical histogram buffers.

Table 1: Datasets used in experiments.

Name	#Train	#Test	#Attribute	Task	Metric
Higgs [2]	10,500,000	500,000	28	Binary	AUC↑
Epsilon ⁵	400,000	100,000	2,000	Binary	AUC↑
Kitsune [21]	14,545,195	3,999,993	115	Binary	AUC↑
Criteo ⁶	41,256,555	4,584,061	67	Binary	AUC↑
Bosch ⁷	1,000,000	183,747	968	Binary	AUC↑
Year [3]	463,715	51,630	90	Regression	RMSE↓
Yahoo LTR ⁸	473,134	165,660	700	Ranking	NDCG@10↑
LETOR [25]	2,270,296	753,611	137	Ranking	NDCG@10↑

6 System Implementation

In this section, we show how to implement quantized GBDT for good efficiency. Current CPU and GPU architectures have limited support for the representation and calculation of low-precision numbers. For example, most CPUs by today only support 8-bit integers as the smallest data type. Under these limitations, the benefits of quantized training cannot be fully exploited. Though the gradients can be compressed into integers with only 2 to 4 bits, we must use at least 8-bit arithmetics for accumulations in histograms. Even with these limitations, we achieve a considerable speedup on existing CPU and GPU architectures, given the techniques introduced in this section.

6.1 Hierarchical Histogram Buffers

Note that in Algorithm 1 most operations are accumulating gradients. Thus, low-bitwidth gradients will not bring much speedup if high-bitwidth integers are used to store the accumulations. On the contrary, integer overflow may occur with low-bitwidth integers storing the accumulations. To maximally exploit low-precision computation resources while avoiding integer overflow, we partition the training dataset by rows (samples) and assign one partition to a thread on CPU or multiple CUDA blocks on GPU. Thus, each thread or CUDA block constructs a local histogram over the samples in the assigned partition. Since the number of training samples per partition is much smaller, in most cases 16-bit integers for the accumulations in the histogram is enough. In the end, local histograms are reduced to the total histogram which may use more bits per bin, e.g. with 16-bit or 32-bit integers. Figure 2 displays this divide-and-merge strategy and how the bitwidths differ in local and total histograms.

6.2 Packed Gradient and Hessian

We pack the summations of gradients and Hessians in a histogram bin into a single integer in a similar way as SecureBoost+ [6]. For example, if we use two 16-bit integers to store the accumulation values, then the packed accumulation value would be a single 32-bit integer. In our case, however, since gradients can be either negative or positive, the accumulation of gradients must reside in the upper part of the packed integer to exploit the signed bit. The accumulation of Hessians resides in the lower part of the packed integer. When accumulating the gradient and Hessian of a sample into a bin, the low-bitwidth gradient and Hessian are packed in the same way before the addition.

Packed gradient and Hessian halves the number of memory accesses in histogram construction. It also halves the number of integer additions. On GPUs, the packing has one more contribution to efficiency. This is because histogram construction on GPUs relies on atomic operations to ensure correctness when multiple threads add to the same histogram. Thus, packing also reduces the overhead of atomic operations.

7 Experiments

We evaluate our quantized GBDT training system on public datasets and compare both accuracy and efficiency with other GBDT tools. First, we show that quantized GBDT training preserves accuracy with low-bitwidth gradients. Then, we assess the efficiency on CPUs and GPU of a single machine,

⁵<https://www.csie.ntu.edu.tw/~cjlin/libsvmtools/datasets/binary.html#epsilon>

⁶<https://go.criteo.net/criteo-research-kaggle-display-advertising-challenge-dataset.tar.gz>

⁷<https://www.kaggle.com/c/bosch-production-line-performance>

⁸<https://webscope.sandbox.yahoo.com/catalog.php?datatype=c>

Table 2: Comparison of accuracy, w.r.t. different quantized bits.

Algorithm	Binary Classification					Regression	Ranking	
	Higgs \uparrow	Epsilon \uparrow	Kitsune \uparrow	Criteo \uparrow	Bosch \uparrow	Year \downarrow	Yahoo LTR \uparrow	LETOR \uparrow
XGBoost	0.845778	0.950210	0.948329	0.802030	0.706423	8.954460	0.794919	0.505058
CatBoost	0.845425	0.943211	0.944557	0.803150	0.687795	8.951745	0.794215	0.519952
LightGBM	0.845694	0.950203	0.950561	0.803791	0.703471	8.956278	0.793792	0.524191
2-bit SR _{refit}	0.845587	0.949472	0.952703	0.803293	0.700040	8.953388	0.788579	0.519067
3-bit SR _{refit}	0.845725	0.949884	0.951309	0.803768	0.702025	8.937374	0.791077	0.522220
4-bit SR _{refit}	0.845507	0.950049	0.950911	0.803783	0.702959	8.942898	0.792664	0.523702
5-bit SR _{refit}	0.845706	0.950298	0.949229	0.803766	0.703242	8.948542	0.793166	0.524616
2-bit SR _{no refit}	0.846713	0.944509	0.952974	0.803750	0.701399	9.112302	0.764862	0.486193
3-bit SR _{no refit}	0.846040	0.949593	0.951385	0.803922	0.702460	8.990034	0.780041	0.507689
4-bit SR _{no refit}	0.845816	0.950127	0.951197	0.803812	0.704053	8.955256	0.787575	0.515767
5-bit SR _{no refit}	0.845842	0.950275	0.949794	0.803790	0.702717	8.952768	0.791631	0.520900
2-bit RN _{refit}	0.795991	0.889149	0.962201	0.779906	0.685407	9.429014	0.765103	0.454512
3-bit RN _{refit}	0.830506	0.944329	0.966606	0.782732	0.688372	9.062854	0.772364	0.476874
4-bit RN _{refit}	0.840747	0.949946	0.961938	0.795803	0.691163	8.968694	0.777347	0.487394
5-bit RN _{refit}	0.843820	0.950457	0.962427	0.802438	0.698529	8.952418	0.784333	0.494828
2-bit RN _{no refit}	0.836683	0.925220	0.946016	0.768338	0.695089	10.685840	0.632058	0.203732
3-bit RN _{no refit}	0.843482	0.946850	0.940961	0.791709	0.697933	9.377560	0.732487	0.350127
4-bit RN _{no refit}	0.845788	0.949676	0.949228	0.802689	0.702767	8.969828	0.765432	0.437317
5-bit RN _{no refit}	0.845765	0.950307	0.952420	0.803645	0.695559	8.965400	0.782608	0.485752

and scalability with distributed training over multiple CPU machines. Ablation study is provided to analyze the techniques for accuracy preservation and system implementation. Table 1 lists the datasets used for the experiments. For Criteo, we encode the categorical features by target and count encoding. We include open-source GBDT tools XGBoost, LightGBM, and CatBoost as baselines. We use the leaf-wise tree-growing strategy [27] for all baselines. A full description of datasets and hyperparameter settings is provided in Appendix C.

7.1 Accuracy of Quantized Training

We evaluate the accuracy of quantized training. For each dataset and each algorithm, the result of the best iteration of the test set is reported. We use gradients with 2-bit, 3-bit, 4-bit and 5-bit integers, and compare the results with 32-bit single-precision FP gradients. Table 2 lists the best metric achieved on the test set across all boosting iterations. We denote stochastic rounding by SR and round-to-nearest by RN. And use the subscripts to indicate whether to apply leaf-value refitting. Here we focus on the effect of quantization on accuracy only (the SR_{refit} part), and leave the discussion of rounding strategy and leaf-value refitting in 7.4.1. And due to limited space, we list only metrics of the CPU version here. Appendix C provides a similar table for GPU version. With low-bitwidth gradients, the accuracy is not affected much. For some datasets, including Epsilon, Yahoo LTR, and LETOR, more gradient bits can improve the performance. Other datasets are less sensitive to the number of bits.

7.2 Speedup on Standalone Machine

We evaluate the acceleration brought by quantized training (SR_{refit}) on a single machine by comparing it with CPU and CUDA implementations of popular open-source GBDT tools. Our quantized training on CPU is based on LightGBM. We compare our CPU implementation with XGBoost, CatBoost, and LightGBM with 32-bit gradients. For the comparison on GPU, we implement a new CUDA version of LightGBM (denoted by LightGBM+, details are in Appendix E) and further implement quantized training based on it. We summarize the benchmark results in Table 3. Overall, quantized training achieves comparable accuracy with a shorter training time. For the histogram construction time, quantized training speeds up histogram construction by up to 3.8 times on GPU, with an overall speedup of up to 2.2 times compared with LightGBM+. We also see the acceleration on the CPU, but with relatively small gains compared with GPU. In summary, quantized training pushes forward the SOTA efficiency of GBDT algorithms. The number of bits for gradients does not influence the training time much. For histogram construction time, we only list the results with 2-bit gradients due to limited space. A full table can be found in Table 6 of Appendix C.

7.3 Speedup of Distributed Training

We evaluate quantization in distributed GBDT training on an enlarged version of the Epsilon dataset, which duplicates 20 copies of the training set of the original Epsilon dataset (denoted by Epsilon-8M),

Table 3: Detailed time costs for different algorithms in different datasets (seconds).

	Algorithm	Higgs	Epsilon	Kitsune	Criteo	Bosch	Year	Yahoo LTR	LETOR
GPU total time	XGBoost	33.97	311.12	181.24	326.82	68.44	20.47	28.64	51.29
	CatBoost	61.10	105.00	80.20	187.80	22.12	33.96	59.22	N/A
	LightGBM+	29.05	87.12	77.43	102.33	21.41	24.33	30.79	41.79
	LightGBM+ 2-bit	24.78	39.04	38.26	61.04	12.57	18.19	23.09	33.60
	LightGBM+ 3-bit	24.45	39.25	38.63	59.93	12.60	18.24	24.93	33.87
	LightGBM+ 4-bit	24.53	39.82	40.00	59.49	12.55	18.34	25.65	34.11
LightGBM+ 5-bit	24.55	41.30	40.83	60.24	12.08	18.41	25.50	34.36	
CPU total time	XGBoost	109.16	1282.97	281.72	565.52	130.92	28.85	103.87	72.37
	CatBoost	1009.8	1283.4	1495.0	7702.2	998.4	95.8	588.2	865.4
	LightGBM	83.27	519.89	332.12	524.61	59.94	12.67	75.44	103.09
	LightGBM 2-bit	73.36	426.50	215.91	444.28	46.63	12.94	61.50	72.08
	LightGBM 3-bit	69.64	459.39	207.96	440.68	47.35	12.79	61.07	74.35
	LightGBM 4-bit	69.30	458.62	208.99	416.60	46.45	11.90	61.15	77.66
LightGBM 5-bit	69.86	457.68	211.53	423.80	47.52	11.79	61.76	77.92	
GPU Hist. time	LightGBM+	11.26	46.96	54.77	70.97	16.57	9.61	11.59	17.75
	LightGBM+ 2-bit	4.84	12.11	16.41	21.74	8.52	4.08	8.23	10.20
CPU Hist. time	LightGBM	50.74	458.46	253.07	385.98	53.08	6.68	58.53	66.39
	LightGBM 2-bit	32.82	375.70	147.10	269.00	39.80	5.99	43.59	38.23

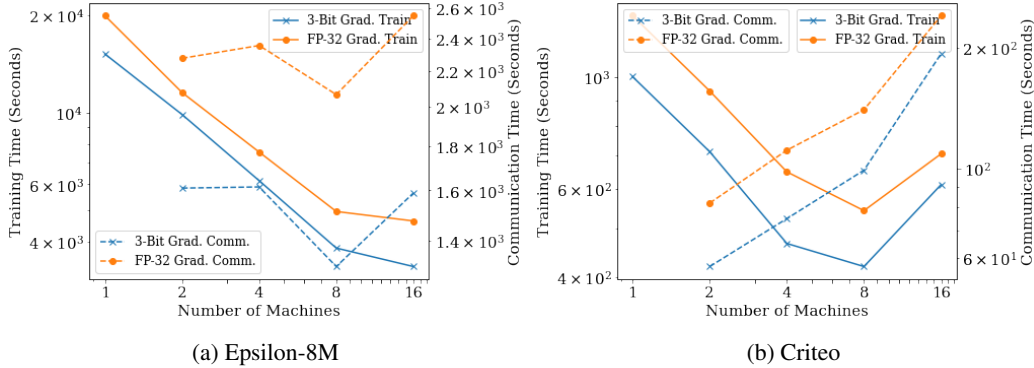


Figure 3: Scaling on distributed systems.

and Criteo. Figure 3 shows how training time and communication time vary with different numbers of machines. Quantization can consistently reduce communication cost and accelerate distributed training. On the Criteo dataset, the communication cost dominates with 16 machines, and the training time with 16 machines is even slower than with 4 machines. This shows that there is still some room for improvement in the scalability of our system.

7.4 Ablation Study

We analyze the effect of proposed techniques that ensure the effectiveness and efficiency of quantized training. We also provide a discussion on the feasibility of the weak-learnability assumption used in Section 5.

7.4.1 Rounding Strategies and Leaf-Value Refitting

Stochastic rounding plays an important role in the accuracy of quantized training. Table 2 also compares the accuracy on test sets with round-to-nearest (denoted by RN) and stochastic rounding (denoted by SR), with different numbers of gradient bits. For both strategies, the results with and without leaf-value refitting are both reported. With smaller numbers of bits, the SR strategy significantly outperforms the RN strategy. Note that leaf-value refitting is not able to compensate for the drawback of the RN. Table 2 also demonstrates how leaf-value refitting influences accuracy. For binary classification, leaf-value refitting is less important as a comparable accuracy could be achieved without it. While for regression and ranking tasks, leaf-value refitting is crucial to achieving comparable accuracy.

7.4.2 Packed Gradient and Hessian

Figure 5 shows the training time and histogram construction time with and without packing gradient and hessian, testing with 2-bit gradients of CPU version. No-packing version on GPU requires atomic addition for 16-bit integers, which is not natively supported by NVIDIA V100 GPUs. Thus, for a clear comparison, we only show the results of CPU version here. Overall, packing is important for the speed of histogram construction.

7.4.3 Histogram Bitwidth

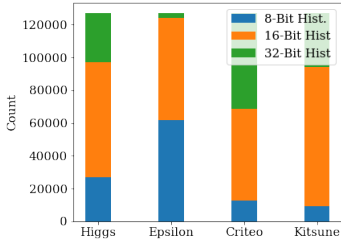


Figure 4: Histogram bitwidth frequency.

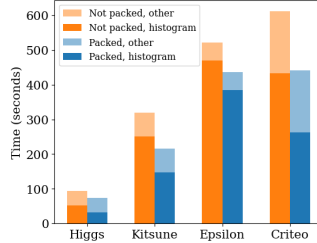


Figure 5: Speedup by packing gradients.

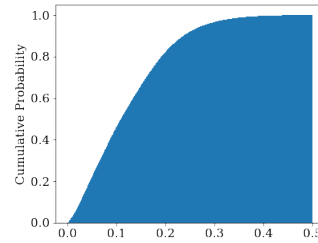


Figure 6: Cumulative distribution of $\hat{\gamma}_s$.

Figure 4 shows the frequency of per-thread histograms of different bitwidths used during training with 2-bit gradients on CPUs. The counts are the number of leaves in the boosting process using the corresponding bitwidth in per-thread histograms. On CPUs, our per-thread histograms can use either 8-bit, 16-bit, or 32-bit integers. For now 8-bit integer histogram is only available with 2-bit gradients in our current version. The bitwidth in histograms is determined by the number of training samples in the leaves, the number of threads/blocks to use, the total number of bins in histograms of all features, and the gradient bitwidth. The minimum bitwidth of histogram integers that won't result in an integer overflow is chosen. The figure shows that quantized training exploits low-precision computations. On GPUs, there's no native support for atomic additions of packed 8-bit integers. Thus, we use 16-bit histograms in CUDA blocks in our current implementation. We leave more aggressive usage of low-bitwidth computations in our future work.

7.4.4 Feasibility of Weak-Learnability Assumption

To verify the feasibility of Assumption 5.2, we should evaluate the largest γ_s with which a stump with weighted classification error rate $\frac{1}{2} - \gamma_s$ exists. This requires enumerating all the splits again and calculating the weighted error rate for each split, which is costing. Luckily, we have an easy approach to obtaining a lower bound of the largest γ_s , which can be naturally recorded during training of GBDT, we name the lower bound as $\hat{\gamma}_s$. $\hat{\gamma}_s$ is the weighted error rate of the optimal split in leaf s according to the criterion in (4). Figure 6 shows the cumulative distribution of $\hat{\gamma}_s$ of all leaves during quantized training of the Year dataset with 3-bit gradients. For most leaves (over 75%), a $\gamma_s > 0.05$ exists. Thus γ_s won't be too small for most leaves.

8 Discussion and Future Work

In this paper, we try to answer an important but previously neglected question: Can GBDT exploit low-precision training? We propose a quantized training framework with low-bitwidth integer arithmetics which enables the low-precision training of GBDT. We identify the key techniques to preserve accuracy with quantized training, including stochastic rounding and leaf-value refitting. Theoretical analysis shows that quantization has a limited impact on the selection of optimal splits in leaves, given enough training data. We implement our algorithm with both CPU and GPU versions. Experiments show that our quantized training GBDT method can achieve comparable accuracy with significant speedup over SOTA GBDT tools, with CPUs, GPUs, and distributed clusters. In this work, we propose a simple stochastic quantization framework. Designing more sophisticated quantization methods for GBDT is an interesting direction for future exploration. We also leave the implementation of quantized GBDT training on multi-GPU distributed systems and more aggressive usage of low-bitwidth computations in our future work. We believe our method will bring new inspirations in improving GBDT training algorithms, as low-precision computation becomes a trend in machine learning.

References

- [1] Firas Abuzaïd, Joseph K Bradley, Feynman T Liang, Andrew Feng, Lee Yang, Matei Zaharia, and Ameet S Talwalkar. Yggdrasil: An optimized system for training deep decision trees at scale. In *Advances in Neural Information Processing Systems*, pages 3817–3825, 2016.
- [2] Pierre Baldi, Peter Sadowski, and Daniel Whiteson. Searching for exotic particles in high-energy physics with deep learning. *Nature communications*, 5(1):1–9, 2014.
- [3] Thierry Bertin-Mahieux, Daniel PW Ellis, Brian Whitman, and Paul Lamere. The million song dataset. 2011.
- [4] Jianfei Chen, Yu Gai, Zhewei Yao, Michael W Mahoney, and Joseph E Gonzalez. A statistical framework for low-bitwidth training of deep neural networks. *Advances in Neural Information Processing Systems*, 33:883–894, 2020.
- [5] Tianqi Chen and Carlos Guestrin. Xgboost: A scalable tree boosting system. In *Proceedings of the 22nd acm sigkdd international conference on knowledge discovery and data mining*, pages 785–794, 2016.
- [6] Weijing Chen, Guoqiang Ma, Tao Fan, Yan Kang, Qian Xu, and Qiang Yang. Secureboost+: A high performance gradient boosting tree framework for large scale vertical federated learning. *arXiv preprint arXiv:2110.10927*, 2021.
- [7] Matthieu Courbariaux, Yoshua Bengio, and Jean-Pierre David. Binaryconnect: Training deep neural networks with binary weights during propagations. In *Advances in neural information processing systems*, pages 3123–3131, 2015.
- [8] Laurens Devos, Wannes Meert, and Jesse Davis. Fast gradient boosting decision trees with bit-level data structures. In *Joint European Conference on Machine Learning and Knowledge Discovery in Databases*, pages 590–606. Springer, 2019.
- [9] Nick Erickson, Jonas Mueller, Alexander Shirkov, Hang Zhang, Pedro Larroy, Mu Li, and Alexander Smola. Autogluon-tabular: Robust and accurate automl for structured data. *arXiv preprint arXiv:2003.06505*, 2020.
- [10] Fangcheng Fu, Yuzheng Hu, Yihan He, Jiawei Jiang, Yingxia Shao, Ce Zhang, and Bin Cui. Don’t waste your bits! squeeze activations and gradients for deep neural networks via tinyscript. In *International Conference on Machine Learning*, pages 3304–3314. PMLR, 2020.
- [11] Fangheng Fu, Jiawei Jiang, Yingxia Shao, and Bin Cui. An experimental evaluation of large scale gbdt systems. *Proceedings of the VLDB Endowment*, 12(11):1357–1370, 2019.
- [12] Alexander Grubb and J Andrew Bagnell. Generalized boosting algorithms for convex optimization. In *Proceedings of the 28th International Conference on International Conference on Machine Learning*, pages 1209–1216, 2011.
- [13] Suyog Gupta, Ankur Agrawal, Kailash Gopalakrishnan, and Pritish Narayanan. Deep learning with limited numerical precision. In *International conference on machine learning*, pages 1737–1746. PMLR, 2015.
- [14] Ziniu Hu, Yang Wang, Qu Peng, and Hang Li. Unbiased lambdamart: An unbiased pairwise learning-to-rank algorithm. In *The World Wide Web Conference*, pages 2830–2836, 2019.
- [15] Itay Hubara, Matthieu Courbariaux, Daniel Soudry, Ran El-Yaniv, and Yoshua Bengio. Binarized neural networks. *Advances in neural information processing systems*, 29, 2016.
- [16] Jiawei Jiang, Bin Cui, Ce Zhang, and Fangcheng Fu. Dimboost: Boosting gradient boosting decision tree to higher dimensions. In *Proceedings of the 2018 International Conference on Management of Data*, pages 1363–1376, 2018.
- [17] Guolin Ke, Qi Meng, Thomas Finley, Taifeng Wang, Wei Chen, Weidong Ma, Qiwei Ye, and Tie-Yan Liu. Lightgbm: A highly efficient gradient boosting decision tree. *Advances in neural information processing systems*, 30:3146–3154, 2017.
- [18] Hao Li, Soham De, Zheng Xu, Christoph Studer, Hanan Samet, and Tom Goldstein. Training quantized nets: A deeper understanding. *Advances in Neural Information Processing Systems*, 30, 2017.
- [19] Qi Meng, Guolin Ke, Taifeng Wang, Wei Chen, Qiwei Ye, Zhi-Ming Ma, and Tie-Yan Liu. A communication-efficient parallel algorithm for decision tree. *Advances in Neural Information Processing Systems*, 29, 2016.
- [20] Paulius Micikevicius, Sharan Narang, Jonah Alben, Gregory Diamos, Erich Elsen, David Garcia, Boris Ginsburg, Michael Houston, Oleksii Kuchaiev, Ganesh Venkatesh, et al. Mixed precision training. In *International Conference on Learning Representations*, 2018.
- [21] Yisroel Mirsky, Tomer Doitshman, Yuval Elovici, and Asaf Shabtai. Kitsune: An ensemble of autoencoders for online network intrusion detection. In *Network and Distributed Systems Security (NDSS) Symposium*, 2018.

- [22] Richard Nock and Robert Williamson. Lossless or quantized boosting with integer arithmetic. In *International Conference on Machine Learning*, pages 4829–4838. PMLR, 2019.
- [23] Phuong Pham, Vivek Jain, Lukas Dauterman, Justin Ormont, and Navendu Jain. Deeptriage: Automated transfer assistance for incidents in cloud services. In *Proceedings of the 26th ACM SIGKDD International Conference on Knowledge Discovery & Data Mining*, pages 3281–3289, 2020.
- [24] Liudmila Prokhorenkova, Gleb Gusev, Aleksandr Vorobev, Anna Veronika Dorogush, and Andrey Gulin. Catboost: unbiased boosting with categorical features. In *Proceedings of the 32nd International Conference on Neural Information Processing Systems*, pages 6639–6649, 2018.
- [25] Tao Qin, Tie-Yan Liu, Jun Xu, and Hang Li. Letor: A benchmark collection for research on learning to rank for information retrieval. *Information Retrieval*, 13(4):346–374, 2010.
- [26] Zhen Qin, Le Yan, Honglei Zhuang, Yi Tay, Rama Kumar Pasumarthi, Xuanhui Wang, Michael Bendersky, and Marc Najork. Are neural rankers still outperformed by gradient boosted decision trees? In *International Conference on Learning Representations*, 2020.
- [27] Haijian Shi. *Best-first decision tree learning*. PhD thesis, The University of Waikato, 2007.
- [28] Qingquan Song, Dehua Cheng, Hanning Zhou, Jiyan Yang, Yuandong Tian, and Xia Hu. Towards automated neural interaction discovery for click-through rate prediction. In *Proceedings of the 26th ACM SIGKDD International Conference on Knowledge Discovery & Data Mining*, pages 945–955, 2020.
- [29] Meng Wan, Chongxin Deng, Siyu Yu, and JD Vectorlab. Diting: A real-time distributed feature serving system for machine learning. Technical report, EasyChair, 2019.
- [30] Wei Wen, Cong Xu, Feng Yan, Chunpeng Wu, Yandan Wang, Yiran Chen, and Hai Li. Terngrad: ternary gradients to reduce communication in distributed deep learning. In *31st International Conference on Neural Information Processing Systems (NIPS 2017)*, 2017.
- [31] Zeyi Wen, Qinbin Li, Bingsheng He, and Bin Cui. Challenges and opportunities of building fast gbdt systems. In *Proceedings of the Thirtieth International Joint Conference on Artificial Intelligence (IJCAI-21) Survey Track*, 2021.
- [32] Lei Yang, Hong Wu, Tieying Zhang, Xuntao Cheng, Feifei Li, Lei Zou, Yujie Wang, Rongyao Chen, Jianying Wang, and Gui Huang. Leaper: a learned prefetcher for cache invalidation in lsm-tree based storage engines. *Proceedings of the VLDB Endowment*, 13(12):1976–1989, 2020.
- [33] Xiao Yang, Daren Sun, Ruiwei Zhu, Tao Deng, Zhi Guo, Zongyao Ding, Shouke Qin, and Yanfeng Zhu. Aiads: Automated and intelligent advertising system for sponsored search. In *Proceedings of the 25th ACM SIGKDD International Conference on Knowledge Discovery & Data Mining*, pages 1881–1890, 2019.
- [34] Huan Zhang, Si Si, and Cho-Jui Hsieh. Gpu-acceleration for large-scale tree boosting. In *SysML Conference*, 2018.
- [35] Shuchang Zhou, Yuxin Wu, Zekun Ni, Xinyu Zhou, He Wen, and Yuheng Zou. Dorefa-net: Training low bitwidth convolutional neural networks with low bitwidth gradients. *CoRR*, abs/1606.06160, 2016.
- [36] Wenjun Zhou, Taposh Dutta Roy, and Iryna Skrypnik. The kdd cup 2019 report. *ACM SIGKDD Explorations Newsletter*, 22(1):8–17, 2020.

Checklist

1. For all authors...
 - (a) Do the main claims made in the abstract and introduction accurately reflect the paper's contributions and scope? [Yes]
 - (b) Did you describe the limitations of your work? [Yes] Our implementation is limited by existing processor architectures, which is discussed in section 6.1
 - (c) Did you discuss any potential negative societal impacts of your work? [No] We believe our method has no negative societal impacts.
 - (d) Have you read the ethics review guidelines and ensured that your paper conforms to them? [Yes]
2. If you are including theoretical results...
 - (a) Did you state the full set of assumptions of all theoretical results? [Yes] All assumptions are strictly stated.
 - (b) Did you include complete proofs of all theoretical results? [Yes] We provide complete and strict proofs in the supplementary.
3. If you ran experiments...
 - (a) Did you include the code, data, and instructions needed to reproduce the main experimental results (either in the supplemental material or as a URL)? [Yes] The data we used are all from public databases.
 - (b) Did you specify all the training details (e.g., data splits, hyperparameters, how they were chosen)? All these details are available in our paper and the appendix. Our source code and processed datasets are publicly available. [Yes]
 - (c) Did you report error bars (e.g., with respect to the random seed after running experiments multiple times)? Our accuracy evaluation in Table 2 are averaged over 5 different runs. [Yes]
 - (d) Did you include the total amount of compute and the type of resources used (e.g., type of GPUs, internal cluster, or cloud provider)? [Yes] Provided in supplementary.
4. If you are using existing assets (e.g., code, data, models) or curating/releasing new assets...
 - (a) If your work uses existing assets, did you cite the creators? [Yes] We discuss all the used datasets in the experiment section
 - (b) Did you mention the license of the assets? [Yes]
 - (c) Did you include any new assets either in the supplemental material or as a URL? [No]
 - (d) Did you discuss whether and how consent was obtained from people whose data you're using/curating? [No] We use publicly available benchmark datasets.
 - (e) Did you discuss whether the data you are using/curating contains personally identifiable information or offensive content? [No] We use publicly available benchmark datasets.
5. If you used crowdsourcing or conducted research with human subjects...
 - (a) Did you include the full text of instructions given to participants and screenshots, if applicable? [N/A] We did not use crowdsourcing or conducted research with human subjects.
 - (b) Did you describe any potential participant risks, with links to Institutional Review Board (IRB) approvals, if applicable? [N/A] We did not use crowdsourcing or conducted research with human subjects.
 - (c) Did you include the estimated hourly wage paid to participants and the total amount spent on participant compensation? [N/A] We did not use crowdsourcing or conducted research with human subjects.

A Summary of Appendix

We provide more details of theoretical analysis (Appendix B and D), experiment results and settings (Appendix C) and a brief introduction to our new implementation of LightGBM CUDA version (Appendix E).

B Theoretical Analysis

For the simplicity of notations, we will use s in place of I_s to represent the indices of data instances in leaf s in this section.

B.1 Existence of $\gamma_s > 0$

Theorem B.1.1 With constant hessian value h , if leaf s has a split gain $\Delta\mathcal{L}_{s \rightarrow s_1, s_2} > 0$, then with weights $|g_i|$ and labels $\text{sign}(g_i)$, there exists $\hat{\gamma}_s > 0$ such that the split $s \rightarrow s_1, s_2$ has a weighted classification error rate $\frac{1}{2} - \hat{\gamma}_s < \frac{1}{2}$ for \mathcal{D}_s .

Proof of Theorem B.1.1 Since

$$\Delta\mathcal{L}_{s \rightarrow s_1, s_2} = \frac{G_{s_1}^2}{2H_{s_1}} + \frac{G_{s_2}^2}{2H_{s_2}} - \frac{G_s^2}{2H_s} = \frac{G_{s_1}^2}{2hn_{s_1}} + \frac{G_{s_2}^2}{2hn_{s_2}} - \frac{G_s^2}{2hn_s} > 0, \quad (10)$$

we have $|G_{s_1}| > 0$ or $|G_{s_2}| > 0$. W.L.O.G., suppose $|G_{s_1}| > 0$. Define s_1^+ as the set of indices such that $\forall i \in s_1^+, \text{sign}(g_i)$ equals the weighted majority of $\text{sign}(g_i)$ for all $i \in s_1$ (weighted by $|g_i|$), and $s_1^- = s_1 - s_1^+$. Then

$$|G_{s_1}| = \left| \sum_{i \in s_1} g_i \right| = \sum_{i \in s_1^+} |g_i| - \sum_{i \in s_1^-} |g_i| > 0. \quad (11)$$

Similarly we define s_2^+ and s_2^- . Then by definition

$$|G_{s_2}| = \left| \sum_{i \in s_2} g_i \right| = \sum_{i \in s_2^+} |g_i| - \sum_{i \in s_2^-} |g_i| \geq 0. \quad (12)$$

Thus the weighted error rate

$$\begin{aligned} \frac{\sum_{i \in s_1^-} |g_i| + \sum_{i \in s_2^-} |g_i|}{\sum_{i \in s_1} |g_i| + \sum_{i \in s_2} |g_i|} &= \frac{1}{2} - \frac{\sum_{i \in s_1^+} |g_i| + \sum_{i \in s_2^+} |g_i| - \sum_{i \in s_1^-} |g_i| - \sum_{i \in s_2^-} |g_i|}{2(\sum_{i \in s_1} |g_i| + \sum_{i \in s_2} |g_i|)} \\ &= \frac{1}{2} - \frac{|G_{s_1}| + |G_{s_2}|}{2(\sum_{i \in s_1} |g_i| + \sum_{i \in s_2} |g_i|)} < \frac{1}{2}. \end{aligned} \quad (13)$$

Setting

$$\hat{\gamma}_s = \frac{|G_{s_1}| + |G_{s_2}|}{2(\sum_{i \in s_1} |g_i| + \sum_{i \in s_2} |g_i|)} > 0 \quad (14)$$

completes the proof.

B.2 Proof of Theorem 5.3

Definition 5.1 (Weak Learnability of Stumps) Given a binary classification dataset $\mathcal{D} = \{(\mathbf{x}_i, c(\mathbf{x}_i))\}_{i=1}^N$ where $c(\mathbf{x}_i) \in \{-1, 1\}$, weights $\{w_i\}_{i=1}^N$, $w_i \geq 0$ and $\sum_i w_i > 0$, there exists $\gamma > 0$ and a two-leaf decision tree with leaf values in $\{-1, 1\}$ s.t. the weighted classification error rate on \mathcal{D} is $\frac{1}{2} - \gamma$. Then the dataset \mathcal{D} is γ -empirically weakly learnable by stumps w.r.t. c and $\{w_i\}_{i=1}^N$.

Assumption 5.2 Let $\text{sign}(\cdot)$ be the sign function (with $\text{sign}(0) = 1$). For data subset $\mathcal{D}_s \subset \mathcal{D}$ in leaf s , there exists a stump and a $\gamma_s > 0$ s.t. \mathcal{D}_s is γ_s -empirically weakly learnable by stumps, w.r.t. concept $c(\mathbf{x}_i) = \text{sign}(g_i)$ and weights $w_i = |g_i|$, where $i \in I_s$.

Theorem 5.3 For loss functions with constant hessian value $h > 0$, if Assumption 5.2 holds for the subset \mathcal{D}_s in leaf s for some $\gamma_s > 0$, then with stochastic rounding and leaf-value refitting, for any $\epsilon > 0$, and $\delta > 0$, at least one of the following conclusions holds:

1. With any split of leaf s and its descendants, the resultant average of absolute values of prediction values by the tree in current boosting iteration for data in \mathcal{D}_s is no greater than ϵ/h .
2. For any split $s \rightarrow s_1, s_2$ of leaf s , with a probability of at least $1 - \delta$,

$$\left| \frac{\tilde{\mathcal{G}}_{s \rightarrow s_1, s_2} - \mathcal{G}_{s \rightarrow s_1, s_2}}{\mathcal{G}_s^*} \right| \leq \frac{\max_{i \in [N]} |g_i| \sqrt{2 \ln \frac{4}{\delta}}}{\gamma_s^2 \epsilon \cdot 2^{B-1}} \left(\sqrt{\frac{1}{n_{s_1}}} + \sqrt{\frac{1}{n_{s_2}}} \right) + \frac{\left(\max_{i \in [N]} |g_i| \right)^2 \ln \frac{4}{\delta}}{\gamma_s^2 \epsilon^2 n_s \cdot 4^{B-2}}. \quad (15)$$

Proof of Theorem 5.3 By leaf-wise weak learnability (Assumption 5.2), there exists a split $s \rightarrow s_L, s_R$ and $\gamma_s > 0$ for s s.t. for data in \mathcal{D}_s , with binary labels $c(\mathbf{x}_i) = \text{sign}(g_i)$ and weights $w_i = |g_i|$, the split results in a stump with weighted binary-classification error rate is $\frac{1}{2} - \gamma_s$. Suppose that in s_L, s_L^+ is the set of weighted majority samples, and s_L^- is the set of weighted minority samples (thus $\text{sign}(g_i) = +1, \forall i \in s_L^+$ and $\text{sign}(g_i) = -1, \forall i \in s_L^-$, or $\text{sign}(g_i) = -1, \forall i \in s_L^+$ and $\text{sign}(g_i) = +1, \forall i \in s_L^-$) such that $\sum_{i \in s_L^+} |g_i| \geq \sum_{i \in s_L^-} |g_i|$. Similarly, we define s_R^+ and s_R^- . Then we have the weighted error rate

$$\overline{\text{err}} = \frac{\sum_{i \in s_L^-} |g_i| + \sum_{i \in s_R^-} |g_i|}{\sum_{i \in s} |g_i|} = \frac{1}{2} - \gamma_s. \quad (16)$$

Thus

$$\frac{\sum_{i \in s_L^+} |g_i| + \sum_{i \in s_R^+} |g_i|}{\sum_{i \in s} |g_i|} = 1 - \overline{\text{err}} = \frac{1}{2} + \gamma_s. \quad (17)$$

Since \mathcal{G}_s^* is for the optimal split in leaf s , we have

$$\begin{aligned} \mathcal{G}_s^* &\geq \mathcal{G}_{s \rightarrow s_L, s_R} = \frac{(\sum_{i \in s_L} g_i)^2}{2h n_{s_L}} + \frac{(\sum_{i \in s_R} g_i)^2}{2h n_{s_R}} \\ &\geq \frac{(|\sum_{i \in s_L} g_i| + |\sum_{i \in s_R} g_i|)^2}{2h (n_{s_L} + n_{s_R})} \\ &= \frac{(\sum_{i \in s_L^+} |g_i| - \sum_{i \in s_L^-} |g_i| + \sum_{i \in s_R^+} |g_i| - \sum_{i \in s_R^-} |g_i|)^2}{2h (n_{s_L} + n_{s_R})} \\ &= \frac{(\sum_{i \in s_L^+ \cup s_R^+} |g_i| - \sum_{i \in s_L^- \cup s_R^-} |g_i|)^2}{2h (n_{s_L} + n_{s_R})} \\ &= \frac{((\frac{1}{2} + \gamma_s) \sum_{i \in s} |g_i| - (\frac{1}{2} - \gamma_s) \sum_{i \in s} |g_i|)^2}{2h (n_{s_L} + n_{s_R})} \\ &= \frac{2\gamma_s^2 (\sum_{i \in s} |g_i|)^2}{h (n_{s_L} + n_{s_R})} = \frac{2\gamma_s^2 (\sum_{i \in s} |g_i|)^2}{h n_s} \end{aligned} \quad (18)$$

If $\frac{\sum_{i \in s} |g_i|}{n_s} \leq \epsilon$, then suppose s'_1, \dots, s'_m are all descendant leaves of s , then the average prediction values by current iteration for data in \mathcal{D}_s in current tree is

$$\frac{\sum_{i=1}^m n_{s'_i} |w_{s'_i}^*|}{\sum_{i=1}^m n_{s'_i}} = \frac{\sum_{i=1}^m |\sum_{i \in s'_i} g_i|}{\sum_{i=1}^m n_{s'_i} h} \leq \frac{\sum_{i \in s} |g_i|}{n_s h} \leq \frac{\epsilon}{h}, \quad (19)$$

which guarantees that the first conclusion holds.

If $\frac{\sum_{i \in s} |g_i|}{n_s} > \epsilon$, let $\epsilon_i = \delta_g \tilde{g}_i - g_i$, thus $|\epsilon_i| \leq \delta_g$ and $\mathbb{E}[\epsilon_i] = 0$. Then

$$\begin{aligned} \left| \tilde{\mathcal{L}}_{s_1}^* - \mathcal{L}_{s_1}^* \right| &= \left| \frac{(\sum_{i \in s_1} g_i + \epsilon_i)^2}{2h n_{s_1}} - \frac{(\sum_{i \in s_1} g_i)^2}{2h n_{s_1}} \right| \\ &= \frac{1}{2h n_{s_1}} \left| \sum_{i \in s_1} 2g_i + \epsilon_i \right| \left| \sum_{i \in s_1} \epsilon_i \right| \leq \frac{1}{2h n_{s_1}} \left(\left| \sum_{i \in s_1} 2g_i \right| \left| \sum_{i \in s_1} \epsilon_i \right| + \left| \sum_{i \in s_1} \epsilon_i \right|^2 \right) \end{aligned} \quad (20)$$

Note that ϵ_i 's are independent random variables. Let $t_{s_1} = \delta_g \sqrt{2n_{s_1} \ln \frac{4}{\delta}}$, then by Hoeffding's inequality,

$$P \left(\left| \sum_{i \in n_{s_1}} \epsilon_i \right| \geq t_{s_1} \right) \leq 2 \exp \left(-\frac{2t_{s_1}^2}{n_{s_1} (2\delta_g)^2} \right) = \frac{\delta}{2}. \quad (21)$$

Then with a probability of at least $1 - \frac{\delta}{2}$

$$\begin{aligned} \left| \tilde{\mathcal{L}}_{s_1}^* - \mathcal{L}_{s_1}^* \right| &\leq \frac{1}{hn_{s_1}} \left(\left| \sum_{i \in s_1} g_i \right| \cdot \delta_g \sqrt{2n_{s_1} \ln \frac{4}{\delta}} + \delta_g^2 n_{s_1} \ln \frac{4}{\delta} \right) \\ &= \frac{\left| \sum_{i \in s_1} g_i \right| \cdot \delta_g \sqrt{\frac{2 \ln \frac{4}{\delta}}{n_{s_1}}} + \frac{\delta_g^2 \ln \frac{4}{\delta}}{h}. \end{aligned} \quad (22)$$

We have

$$\begin{aligned} \frac{\left| \sum_{i \in s_1} g_i \right| \cdot \delta_g \sqrt{\frac{2 \ln \frac{4}{\delta}}{n_{s_1}}}}{h\mathcal{G}_s^*} &\leq \frac{\sum_{i \in s_1} |g_i| \cdot \delta_g \sqrt{\frac{2 \ln \frac{4}{\delta}}{n_{s_1}}}}{\frac{2\gamma_s^2 (\sum_{i \in s} |g_i|)^2}{n_s}} \leq \frac{\delta_g \sqrt{\frac{2 \ln \frac{4}{\delta}}{n_{s_1}}}}{\frac{2\gamma_s^2 (\sum_{i \in s} |g_i|)}{n_s}} \\ &\leq \frac{\delta_g \sqrt{\frac{2 \ln \frac{4}{\delta}}{n_{s_1}}}}{2\gamma_s^2 \epsilon} = \frac{\max_{i \in [N]} |g_i|}{2\gamma_s^2 \epsilon (2^{B-1} - 1)} \sqrt{\frac{2 \ln \frac{4}{\delta}}{n_{s_1}}}. \end{aligned} \quad (23)$$

And since

$$\mathcal{G}_s^* \geq \frac{2\gamma_s^2 (\sum_{i \in s} |g_i|)^2}{hn_s} > \frac{2\gamma_s^2 \epsilon^2 n_s}{h}, \quad (24)$$

we have

$$\frac{\delta_g^2 \ln \frac{4}{\delta}}{h\mathcal{G}_s^*} \leq \frac{\delta_g^2 \ln \frac{4}{\delta}}{2\gamma_s^2 \epsilon^2 n_s} = \frac{(\max_{i \in [N]} |g_i|)^2 \ln \frac{4}{\delta}}{2\gamma_s^2 \epsilon^2 (2^{B-1} - 1)^2 n_s}. \quad (25)$$

Thus with a probability of at least $1 - \frac{\delta}{2}$,

$$\begin{aligned} \frac{\left| \tilde{\mathcal{L}}_{s_1}^* - \mathcal{L}_{s_1}^* \right|}{\mathcal{G}_s^*} &\leq \frac{\max_{i \in [N]} |g_i|}{2\gamma_s^2 \epsilon (2^{B-1} - 1)} \sqrt{\frac{2 \ln \frac{4}{\delta}}{n_{s_1}}} + \frac{(\max_{i \in [N]} |g_i|)^2 \ln \frac{4}{\delta}}{2\gamma_s^2 \epsilon^2 (2^{B-1} - 1)^2 n_s} \\ &\leq \frac{\max_{i \in [N]} |g_i|}{\gamma_s^2 \epsilon \cdot 2^{B-1}} \sqrt{\frac{2 \ln \frac{4}{\delta}}{n_{s_1}}} + \frac{(\max_{i \in [N]} |g_i|)^2 \ln \frac{4}{\delta}}{2\gamma_s^2 \epsilon^2 n_s \cdot 4^{B-2}} \end{aligned} \quad (26)$$

Similarly, with a probability of at least $1 - \frac{\delta}{2}$

$$\frac{\left| \tilde{\mathcal{L}}_{s_2}^* - \mathcal{L}_{s_2}^* \right|}{\mathcal{G}_s^*} \leq \frac{\max_{i \in [N]} |g_i|}{\gamma_s^2 \epsilon \cdot 2^{B-1}} \sqrt{\frac{2 \ln \frac{4}{\delta}}{n_{s_2}}} + \frac{(\max_{i \in [N]} |g_i|)^2 \ln \frac{4}{\delta}}{2\gamma_s^2 \epsilon^2 n_s \cdot 4^{B-2}} \quad (27)$$

By union bound, with a probability of at least $1 - \delta$

$$\begin{aligned} \frac{\left| \tilde{\mathcal{G}}_{s \rightarrow s_1, s_2} - \mathcal{G}_{s \rightarrow s_1, s_2} \right|}{\mathcal{G}_s^*} &\leq \frac{\left| \tilde{\mathcal{L}}_{s_1}^* - \mathcal{L}_{s_1}^* \right| + \left| \tilde{\mathcal{L}}_{s_2}^* - \mathcal{L}_{s_2}^* \right|}{\mathcal{G}_s^*} \\ &\leq \frac{\max_{i \in [N]} |g_i| \sqrt{2 \ln \frac{4}{\delta}}}{\gamma_s^2 \epsilon \cdot 2^{B-1}} \left(\sqrt{\frac{1}{n_{s_1}}} + \sqrt{\frac{1}{n_{s_2}}} \right) + \frac{(\max_{i \in [N]} |g_i|)^2 \ln \frac{4}{\delta}}{\gamma_s^2 \epsilon^2 n_s \cdot 4^{B-2}} \end{aligned} \quad (28)$$

B.3 Loss Functions with Non-constant Hessians

Commonly used loss functions for binary-classification, multi-classification, and ranking have non-constant hessian values. Note that all these loss functions have non-negative hessian values. We analyze the error caused by quantization for these functions in this section. Let $\bar{h}_s = \frac{\sum_{i \in s} h_i}{n_s}$ to be the average of hessian values in leaf s . We have the following theorem.

Theorem B.3.1 For loss functions with non-constant hessian values, if Assumption 5.2 holds for the subset \mathcal{D}_s in leaf s for some $\gamma_s > 0$, then with stochastic rounding and leaf-value refitting, for any $\epsilon > 0$ and $\delta > 0$, at least one of the following conclusions holds:

1. With any split of leaf s and its descendants, the resultant weighted average (weighted by h_i) of absolute values of prediction values by the tree in current boosting iteration for data in \mathcal{D}_s is no greater than ϵ .
2. For any split $s \rightarrow s_1, s_2$ of leaf s , if $n_{s_1} \geq \frac{8\delta_h^2 \ln 8/\delta}{\bar{h}_{s_1}^2}$ and $n_{s_2} \geq \frac{8\delta_h^2 \ln 8/\delta}{\bar{h}_{s_2}^2}$, i.e. $n_{s_1} \leq \frac{(\sum_{i \in s_1} h_i)^2}{8\delta_h^2 \ln 8/\delta}$ and $n_{s_2} \leq \frac{(\sum_{i \in s_2} h_i)^2}{8\delta_h^2 \ln 8/\delta}$, then with a probability of at least $1 - \delta$

$$\begin{aligned} \frac{|\tilde{\mathcal{G}}_{s \rightarrow s_1, s_2} - \mathcal{G}_{s \rightarrow s_1, s_2}|}{\mathcal{G}_s^*} &\leq \frac{\delta_g \sqrt{2 \ln 8/\delta}}{\gamma_s^2 \epsilon} \left(\frac{1}{\bar{h}_{s_1} \sqrt{n_{s_1}}} + \frac{1}{\bar{h}_{s_2} \sqrt{n_{s_2}}} \right) \\ &\quad + \frac{\bar{h}_s \delta_h \sqrt{2 \ln 8/\delta}}{2\gamma_s^2} \left(\frac{n_s}{\bar{h}_{s_1}^2 n_{s_1} \sqrt{n_{s_1}}} + \frac{n_s}{\bar{h}_{s_2}^2 n_{s_2} \sqrt{n_{s_2}}} \right) \\ &\quad + \frac{\delta_g^2 \ln 8/\delta}{\gamma_s^2 \bar{h}_s \epsilon^2} \left(\frac{1}{\bar{h}_{s_1} n_s} + \frac{1}{\bar{h}_{s_2} n_s} \right) \end{aligned} \quad (29)$$

Proof of Theorem B.3.1 By leaf-wise weak learnability (Assumption 5.2), there exists a split $s \rightarrow s_L, s_R$ and $\gamma_s > 0$ for s s.t. for data in \mathcal{D}_s , with binary labels $c(\mathbf{x}_i) = \text{sign}(g_i)$ and weights $w_i = |g_i|$, the split results in a stump with weighted binary-classification error is $\frac{1}{2} - \gamma_s$. Similar to the case of loss functions with constant hessian, we define s_L^+, s_L^-, s_R^+ and s_R^- , and first derive a lower bound for \mathcal{G}_s^* ,

$$\begin{aligned} \mathcal{G}_s^* &\geq \mathcal{G}_{s \rightarrow s_L, s_R} = \frac{(\sum_{i \in s_L} g_i)^2}{2 \sum_{i \in s_L} h_i} + \frac{(\sum_{i \in s_R} g_i)^2}{2 \sum_{i \in s_R} h_i} \\ &\geq \frac{(|\sum_{i \in s_L} g_i| + |\sum_{i \in s_R} g_i|)^2}{2 \sum_{i \in s} h_i} \\ &= \frac{(\sum_{i \in s_L^+} |g_i| - \sum_{i \in s_L^-} |g_i| + \sum_{i \in s_R^+} |g_i| - \sum_{i \in s_R^-} |g_i|)^2}{2 \sum_{i \in s} h_i} \\ &= \frac{(\sum_{i \in s_L^+ \cup s_R^+} |g_i| - \sum_{i \in s_L^- \cup s_R^-} |g_i|)^2}{2 \sum_{i \in s} h_i} \\ &= \frac{((\frac{1}{2} + \gamma_s) \sum_{i \in s} |g_i| - (\frac{1}{2} - \gamma_s) \sum_{i \in s} |g_i|)^2}{2 \sum_{i \in s} h_i} \\ &= \frac{2\gamma_s^2 (\sum_{i \in s} |g_i|)^2}{\sum_{i \in s} h_i} \end{aligned} \quad (30)$$

Let $\xi_i = \delta_h \tilde{h}_i - h_i$ and $\epsilon_i = \delta_g \tilde{g}_i - g_i$, thus $|\xi_i| \leq \delta_h$, $|\epsilon_i| \leq \delta_g$, $\mathbb{E}[\xi_i] = 0$ and $\mathbb{E}[\epsilon_i] = 0$. We then bound the error of $\sum_{i \in s_1} h_i$,

$$\left| \sum_{i \in s_1} (h_i + \xi_i) - \sum_{i \in s_1} h_i \right| = \left| \sum_{i \in s_1} \xi_i \right|. \quad (31)$$

Note that ξ_i 's and ϵ_i 's are independent variables. Let $t'_{s_1} = \delta_h \sqrt{2n_{s_1} \ln \frac{8}{\delta}}$, then by Hoeffding's inequality,

$$P\left(\left|\sum_{i \in s_1} \xi_i\right| \geq t'_{s_1}\right) \leq 2 \exp\left(-\frac{2t'_{s_1}{}^2}{n_{s_1}(2\delta_h)^2}\right) = \frac{\delta}{4} \quad (32)$$

Similarly, let $t''_{s_1} = \delta_g \sqrt{2n_{s_1} \ln \frac{8}{\delta}}$, then by Hoeffding's inequality we can bound the error of $\sum_{i \in s_1} g_i$,

$$P\left(\left|\sum_{i \in s_1} \epsilon_i\right| \geq t''_{s_1}\right) \leq 2 \exp\left(-\frac{2t''_{s_1}{}^2}{n_{s_1}(2\delta_g)^2}\right) = \frac{\delta}{4} \quad (33)$$

If $\frac{\sum_{i \in s} |g_i|}{\sum_{i \in s} h_i} \leq \epsilon$, then suppose s'_1, \dots, s'_m are all descendant leaves of s , then the average (weighted by h_i 's) prediction value for data in \mathcal{D}_s in current tree is

$$\frac{\sum_{i=1}^m \sum_{i \in s'_i} h_i |w_{s'_i}^*|}{\sum_{i=1}^m \sum_{i \in s'_i} h_i} = \frac{\sum_{i=1}^m \left|\sum_{i \in s'_i} g_i\right|}{\sum_{i=1}^m \sum_{i \in s'_i} h_i} \leq \frac{\sum_{i \in s} |g_i|}{\sum_{i \in s} h_i} \leq \epsilon \quad (34)$$

which guarantees that the first conclusion holds.

If $\frac{\sum_{i \in s} |g_i|}{\sum_{i \in s} h_i} > \epsilon$, then we denote $\bar{h}_{s_1} = \frac{\sum_{i \in s_1} h_i}{n_{s_1}}$. If $n_{s_1} \geq \frac{8\delta_h^2 \ln 8/\delta}{\bar{h}_{s_1}^2}$, i.e. $n_{s_1} \leq \frac{(\sum_{i \in s_1} h_i)^2}{8\delta_h^2 \ln 8/\delta}$, then we have $\left|\sum_{i \in s_1} \xi_i\right| \leq \frac{\sum_{i \in s_1} h_i}{2}$ with a probability of at least $1 - \frac{\delta}{4}$ by equation (32). Thus with a probability of at least $1 - \frac{\delta}{2}$,

$$\begin{aligned} \left|\tilde{\mathcal{L}}_{s_1}^* - \mathcal{L}_{s_1}^*\right| &= \frac{1}{2} \left| \frac{(\sum_{i \in s_1} g_i + \epsilon_i)^2}{\sum_{i \in s_1} h_i + \xi_i} - \frac{(\sum_{i \in s_1} g_i)^2}{\sum_{i \in s_1} h_i} \right| \\ &= \frac{1}{2} \left| \frac{(\sum_{i \in s_1} g_i + \epsilon_i)^2 (\sum_{i \in s_1} h_i) - (\sum_{i \in s_1} h_i + \xi_i) (\sum_{i \in s_1} g_i)^2}{(\sum_{i \in s_1} h_i + \xi_i) (\sum_{i \in s_1} h_i)} \right| \\ &\leq \frac{\left| (\sum_{i \in s_1} g_i + \epsilon_i)^2 (\sum_{i \in s_1} h_i) - (\sum_{i \in s_1} g_i)^2 (\sum_{i \in s_1} h_i) \right|}{2 (\sum_{i \in s_1} h_i + \xi_i) (\sum_{i \in s_1} h_i)} \\ &\quad + \frac{\left| (\sum_{i \in s_1} g_i)^2 (\sum_{i \in s_1} h_i) - (\sum_{i \in s_1} g_i)^2 (\sum_{i \in s_1} h_i + \xi_i) \right|}{2 (\sum_{i \in s_1} h_i + \xi_i) (\sum_{i \in s_1} h_i)} \\ &\leq \frac{|\sum_{i \in s_1} \epsilon_i| |\sum_{i \in s_1} g_i|}{\sum_{i \in s_1} h_i + \xi_i} + \frac{|\sum_{i \in s_1} \epsilon_i|^2}{2 (\sum_{i \in s_1} h_i + \xi_i)} + \frac{(\sum_{i \in s_1} g_i)^2 |\sum_{i \in s_1} \xi_i|}{2 (\sum_{i \in s_1} h_i + \xi_i) (\sum_{i \in s_1} h_i)} \\ &\leq \frac{2 |\sum_{i \in s_1} \epsilon_i| |\sum_{i \in s_1} g_i|}{\sum_{i \in s_1} h_i} + \frac{|\sum_{i \in s_1} \epsilon_i|^2}{\sum_{i \in s_1} h_i} + \frac{(\sum_{i \in s_1} g_i)^2 |\sum_{i \in s_1} \xi_i|}{(\sum_{i \in s_1} h_i)^2} \end{aligned} \quad (35)$$

Because

$$\frac{2 |\sum_{i \in s_1} \epsilon_i| |\sum_{i \in s_1} g_i|}{\mathcal{G}_s^* \sum_{i \in s_1} h_i} \leq \frac{(\sum_{i \in s} h_i) |\sum_{i \in s_1} \epsilon_i| |\sum_{i \in s_1} g_i|}{\gamma_s^2 (\sum_{i \in s} |g_i|)^2 \sum_{i \in s_1} h_i} \leq \frac{|\sum_{i \in s_1} \epsilon_i|}{\gamma_s^2 \bar{h}_{s_1} \epsilon n_{s_1}} \leq \frac{\delta_g \sqrt{2 \ln 8/\delta}}{\gamma_s^2 \bar{h}_{s_1} \epsilon \sqrt{n_{s_1}}}, \quad (36)$$

$$\frac{|\sum_{i \in s_1} \epsilon_i|^2}{\mathcal{G}_s^* \sum_{i \in s_1} h_i} \leq \frac{(\sum_{i \in s} h_i) |\sum_{i \in s_1} \epsilon_i|^2}{2\gamma_s^2 (\sum_{i \in s} |g_i|)^2 \sum_{i \in s_1} h_i} \leq \frac{|\sum_{i \in s_1} \epsilon_i|^2}{2\gamma_s^2 \bar{h}_s \bar{h}_{s_1} \epsilon^2 n_s n_{s_1}} \leq \frac{\delta_g^2 \ln 8/\delta}{\gamma_s^2 \bar{h}_s \bar{h}_{s_1} \epsilon^2 n_s}, \quad (37)$$

$$\frac{(\sum_{i \in s_1} g_i)^2 |\sum_{i \in s_1} \xi_i|}{\mathcal{G}_s^* (\sum_{i \in s_1} h_i)^2} \leq \frac{n_s \bar{h}_s |\sum_{i \in s_1} \xi_i|}{2\gamma_s^2 (\sum_{i \in s_1} h_i)^2} \leq \frac{n_s \bar{h}_s \delta_h \sqrt{2 \ln 8/\delta}}{2\gamma_s^2 \bar{h}_{s_1}^2 n_{s_1} \sqrt{n_{s_1}}}. \quad (38)$$

Thus with probability at least $1 - \frac{\delta}{2}$ we have

$$\frac{|\tilde{\mathcal{L}}_{s_1}^* - \mathcal{L}_{s_1}^*|}{\mathcal{G}_s^*} \leq \frac{\sqrt{2 \ln 8/\delta}}{\gamma_s^2} \left(\frac{\delta_g}{\bar{h}_{s_1} \epsilon \sqrt{n_{s_1}}} + \frac{\bar{h}_s \delta_h n_s}{2 \bar{h}_{s_1}^2 n_{s_1} \sqrt{n_{s_1}}} \right) + \frac{\delta_g^2 \ln 8/\delta}{\gamma_s^2 \bar{h}_s \bar{h}_{s_1} \epsilon^2 n_s}. \quad (39)$$

Similarly with probability at least $1 - \frac{\delta}{2}$ we have

$$\frac{|\tilde{\mathcal{L}}_{s_2}^* - \mathcal{L}_{s_2}^*|}{\mathcal{G}_s^*} \leq \frac{\sqrt{2 \ln 8/\delta}}{\gamma_s^2} \left(\frac{\delta_g}{\bar{h}_{s_2} \epsilon \sqrt{n_{s_2}}} + \frac{\bar{h}_s \delta_h n_s}{2 \bar{h}_{s_2}^2 n_{s_2} \sqrt{n_{s_2}}} \right) + \frac{\delta_g^2 \ln 8/\delta}{\gamma_s^2 \bar{h}_s \bar{h}_{s_2} \epsilon^2 n_s}. \quad (40)$$

And finally, with probability at least $1 - \delta$,

$$\begin{aligned} \frac{|\tilde{\mathcal{G}}_{s \rightarrow s_1, s_2} - \mathcal{G}_{s \rightarrow s_1, s_2}|}{\mathcal{G}_s^*} &\leq \frac{\delta_g \sqrt{2 \ln 8/\delta}}{\gamma_s^2 \epsilon} \left(\frac{1}{\bar{h}_{s_1} \sqrt{n_{s_1}}} + \frac{1}{\bar{h}_{s_2} \sqrt{n_{s_2}}} \right) \\ &\quad + \frac{\bar{h}_s \delta_h \sqrt{2 \ln 8/\delta}}{2 \gamma_s^2} \left(\frac{n_s}{\bar{h}_{s_1}^2 n_{s_1} \sqrt{n_{s_1}}} + \frac{n_s}{\bar{h}_{s_2}^2 n_{s_2} \sqrt{n_{s_2}}} \right) \\ &\quad + \frac{\delta_g^2 \ln 8/\delta}{\gamma_s^2 \bar{h}_s \epsilon^2} \left(\frac{1}{\bar{h}_{s_1} n_s} + \frac{1}{\bar{h}_{s_2} n_s} \right). \end{aligned} \quad (41)$$

C Experiment Details

In this section, we provide more details about the results, experiment environments, and hyperparameter settings.

C.1 Variance of Quantized Training

In Table 2 the metric values are averaged over 5 random seeds. The seeds are used to generate random numbers for stochastic rounding. We omit the standard deviation in Table 2 due to limited space. Here we provide a full table with standard deviation listed in Table 4. Note that we report the metric on the best iteration in the test sets. As we can see the variance caused by stochastic rounding in quantization is small, and quantized training is quite stable with different random seeds.

C.2 Accuracy of Quantized Training on GPU

Table 5 shows the accuracy of quantized training on GPU, averaged over 5 random seeds for stochastic rounding with leaf-value refitting. For the GPU version, we run up to 5 bits for gradient discretization. As we can see, for most datasets a comparable performance is achieved with quantized training. Note that we report the metric on the best iteration in the test sets.

C.3 Detailed Training Time

Table 6 shows the detailed training time records. Note that training time numbers are evaluated with 5 random seeds. Time for data loading and pre-processing is excluded. When recording training time, all metric evaluations are disabled. For quantized training, the number of bits does not influence the training time much. This indicates that more acceleration can be achieved for low-bitwidth gradients like 2-bit or 3-bit, with better hardware support for operations of low-bitwidth integers.

C.4 Experiment Environments

Table 7 and 8 list the experiment environments used in this paper for standalone machines. For CPU clusters in distributed experiments, we use 16 nodes each with one Intel(R) Xeon(R) CPU E5-2673 v4 or Intel(R) Xeon(R) Platinum 8171M CPU. The nodes are connected by a network of bandwidth between $7 \sim 8\text{Gbps}$ (tested with iperf⁹).

⁹<https://iperf.fr/>

Table 4: Accuracy with standard variance, w.r.t. different quantized bits (CPU version).

Algorithm	Binary Classification					Regression	Ranking	
	Higgs \uparrow	Epsilon \uparrow	Kitsune \uparrow	Criteo \uparrow	Bosch \uparrow	Year \downarrow	Yahoo LTR \uparrow	LETOR \uparrow
XGBoost	0.845778 \pm .000000	0.950210 \pm .000000	0.948329 \pm .000000	0.802030 \pm .000000	0.706423 \pm .000000	8.954460 \pm .000000	0.794919 \pm .000000	0.505058 \pm .000000
CatBoost	0.845425 \pm .000144	0.943211 \pm .000073	0.944557 \pm .008969	0.803150 \pm .000232	0.687795 \pm .000282	8.951745 \pm .005324	0.794215 \pm .000196	0.519952 \pm .000568
LightGBM	0.845694 \pm .000162	0.950203 \pm .000144	0.950561 \pm .000638	0.803791 \pm .000052	0.703471 \pm .001110	8.956278 \pm .004803	0.793792 \pm .000259	0.524191 \pm .000360
2-bit SR _{refit}	0.845587 \pm .000042	0.949472 \pm .000166	0.952703 \pm .000729	0.803293 \pm .000091	0.700040 \pm .001759	8.953388 \pm .012679	0.788579 \pm .000357	0.519067 \pm .000681
3-bit SR _{refit}	0.845725 \pm .000193	0.949884 \pm .000095	0.951309 \pm .001352	0.803768 \pm .000050	0.702025 \pm .001519	8.937374 \pm .007487	0.791077 \pm .000894	0.522220 \pm .000721
4-bit SR _{refit}	0.845507 \pm .000127	0.950049 \pm .000072	0.950911 \pm .001557	0.803783 \pm .000073	0.702959 \pm .000607	8.942898 \pm .008327	0.792664 \pm .000467	0.523702 \pm .000653
5-bit SR _{refit}	0.845706 \pm .000171	0.950298 \pm .000108	0.949229 \pm .001964	0.803766 \pm .000053	0.703242 \pm .001041	8.948542 \pm .003732	0.793166 \pm .000487	0.524616 \pm .000439
2-bit SR _{no refit}	0.846713 \pm .000184	0.944509 \pm .000174	0.952974 \pm .001024	0.803750 \pm .000068	0.701399 \pm .001663	9.112302 \pm .014516	0.764862 \pm .000858	0.486193 \pm .001789
3-bit SR _{no refit}	0.846040 \pm .000178	0.949593 \pm .000119	0.951385 \pm .001158	0.803922 \pm .000064	0.702460 \pm .000768	8.990034 \pm .009847	0.780041 \pm .000618	0.507689 \pm .001126
4-bit SR _{no refit}	0.845816 \pm .000304	0.950127 \pm .000172	0.951197 \pm .001067	0.803812 \pm .000074	0.704053 \pm .000277	8.955256 \pm .003074	0.787575 \pm .001173	0.515767 \pm .000448
5-bit SR _{no refit}	0.845842 \pm .000119	0.950275 \pm .000234	0.949794 \pm .002275	0.803790 \pm .000096	0.702717 \pm .001075	8.952768 \pm .009403	0.791631 \pm .000590	0.520900 \pm .001087
2-bit RN _{refit}	0.795991 \pm .000582	0.889149 \pm .000856	0.962201 \pm .000820	0.779906 \pm .000323	0.685407 \pm .001055	9.429014 \pm .017197	0.765103 \pm .000918	0.454512 \pm .005565
3-bit RN _{refit}	0.830506 \pm .000495	0.944329 \pm .000319	0.966606 \pm .001074	0.782732 \pm .000210	0.688372 \pm .000351	9.062854 \pm .014744	0.772364 \pm .000822	0.476874 \pm .001500
4-bit RN _{refit}	0.840747 \pm .000241	0.949946 \pm .000207	0.961938 \pm .001970	0.795803 \pm .000099	0.691163 \pm .000698	8.968694 \pm .005092	0.777347 \pm .000969	0.487394 \pm .003279
5-bit RN _{refit}	0.843820 \pm .000073	0.950457 \pm .000071	0.962427 \pm .001150	0.802438 \pm .000083	0.698529 \pm .000425	8.952418 \pm .003649	0.784333 \pm .000612	0.494828 \pm .001543
2-bit RN _{no refit}	0.836683 \pm .000468	0.925220 \pm .001545	0.946016 \pm .005072	0.768338 \pm .000202	0.695089 \pm .001510	10.685840 \pm .001819	0.632058 \pm .005683	0.203732 \pm .005507
3-bit RN _{no refit}	0.843482 \pm .000306	0.946850 \pm .000399	0.940961 \pm .006586	0.791709 \pm .000379	0.697933 \pm .001424	9.377560 \pm .042545	0.732487 \pm .001121	0.350127 \pm .004163
4-bit RN _{no refit}	0.845788 \pm .000176	0.949676 \pm .000126	0.949228 \pm .002973	0.802689 \pm .000096	0.702767 \pm .000408	8.969828 \pm .005646	0.765432 \pm .000426	0.437317 \pm .001514
5-bit RN _{no refit}	0.845765 \pm .000248	0.950307 \pm .000150	0.952420 \pm .003838	0.803645 \pm .000102	0.695559 \pm .000582	8.965400 \pm .002101	0.782608 \pm .000514	0.485752 \pm .001105

C.5 Hyperparameter Settings

For all accuracy and training time evaluations in this paper, we use the hyperparameters of LightGBM, XGBoost, and Catboost as listed in Table 9, 10, and 11, except for the Bosch dataset. For the Bosch dataset, we use learning_rate 0.015 for LightGBM and CatBoost, eta 0.015 for XGBoost, num_leaves 45 for LightGBM, max_leaves 45 for XGBoost and CatBoost, and keep other hyperparameters the same as in the tables. The hyperparameters are chosen so that all these algorithms have similar tree sizes for a fair comparison of training time. In addition, since our GPU machine has 24 physical CPU cores, we set the number of threads of all experiments on GPU to be 24. For training time of LightGBM on CPU, we use force_col_wise=true mode For Bosch, Yahoo LTR, Year, and Epsilon (except 2-bit and 3-bit quantized training). For all other cases we use force_row_wise=true mode of LightGBM CPU version.

The git commit used for CatBoost is 2617a690c77c9c8da1c22d1750b5fbc0eb0eb36d (Date: Thu Jan 12 05:29:47 2023 +0300). And for XGBoost it is cfa994d57fb713e203a494319a6d33fcd007adf8 (Date: Wed Jan 11 05:51:14 2023 +0800). For LightGBM, we use the commit 5df7d516f3e64e8431aecfea892a850afef787bb (Date: Fri Jan 13 17:02:42 2023 +0200) for the FP32 experiments on CPU. For other experiments of LightGBM, we use the version provided in our Github link <https://github.com/Quantized-GBDT/Quantized-GBDT>.

Table 5: Accuracy with standard variance, w.r.t. different quantized bits (GPU version).

Algorithm	Binary-Class					Regression	Ranking	
	Higgs↑	Epsilon↑	Kitsune↑	Criteo↑	Bosch↑	Year↓	Yahoo LTR↑	LETOR↑
XGBoost	0.846035 ±.000000	0.950305 ±.000000	0.949952 ±.000000	0.802159 ±.000000	0.705095 ±.000000	8.949647 ±.000000	0.794026 ±.000000	0.506957 ±.000000
CatBoost	0.845237 ±.000211	0.949214 ±.000115	0.953293 ±.001535	0.803766 ±.000083	0.713931 ±.000685	8.968944 ±.004703	0.794176 ±.000175	N/A
LightGBM+	0.845729 ±.000081	0.950228 ±.000110	0.955914 ±.000962	0.803805 ±.000122	0.703479 ±.001100	8.956194 ±.004720	0.794892 ±.000688	0.526611 ±.000614
2-bit SR _{refit}	0.846582 ±.000159	0.945205 ±.000255	0.952898 ±.001554	0.803594 ±.000077	0.700896 ±.001099	9.107948 ±.007273	0.769811 ±.000495	0.492340 ±.001090
3-bit SR _{refit}	0.845877 ±.000255	0.949494 ±.000277	0.951672 ±.002186	0.803847 ±.000059	0.702262 ±.000903	8.980230 ±.006827	0.784282 ±.000535	0.511955 ±.001200
4-bit SR _{refit}	0.845872 ±.000199	0.950176 ±.000066	0.951918 ±.001138	0.803799 ±.000089	0.703318 ±.001258	8.962148 ±.016629	0.790682 ±.000536	0.519747 ±.000716
5-bit SR _{refit}	0.845849 ±.000238	0.950177 ±.000174	0.950538 ±.000354	0.803827 ±.000095	0.703152 ±.000360	8.953900 ±.004574	0.793978 ±.000490	0.523701 ±.000390

C.6 Data Split and Preprocessing

For most datasets (Higgs, Epsilon, Yahoo, LETOR, Year, Bosch) we use the convention in previous works or the default split [34, 25, 3], without additional preprocessing. For Criteo, we encode the categorical features in the original dataset with target and count encoding. We use the `train.txt` file of the Kaggle version of the Criteo dataset, with the first 41, 256, 555 rows as the training set and the last 4, 584, 061 rows as the test set. For Kitsune, we select the first 80% packets in each attack method to form the training set, and the final 20% packets to form the test set. The datasets can be freely downloaded from <https://pretrain.blob.core.windows.net/quantized-gbdt/dataset.zip>.

D Discussion on Loss Functions with Non-constant Hessians

Appendix B.3 provides the theoretical analysis and proof for the error caused by quantization for loss functions with non-constant Hessians. The assumption is a little bit stronger than constant hessian loss functions in that we are expecting the average hessian values per leaf won't be too small, so that $n_{s_1} \geq \frac{8\delta_h^2 \ln 8/\delta}{\bar{h}_{s_1}}$ and $n_{s_2} \geq \frac{8\delta_h^2 \ln 8/\delta}{\bar{h}_{s_2}}$ hold. Figure 7 shows the average hessian values in each iteration with 3-bit gradients. We first calculate the average hessian values for all leaves in each iteration. Then we plot the mean of the average hessian values over the leaves in each iteration in solid blue curves, with the shadow area indicating the range between 10% and 90% percentiles over the leaves in each iteration. For most leaves, the average hessian values are not too small. And it is easy to meet the condition $n_s \geq \frac{8\delta_h^2 \ln 8/\delta}{\bar{h}_s}$ with enough training data. For example, suppose $\bar{h}_s = 0.01$, then for binary classification, with 3-bit gradients, $\delta_h = \frac{0.25}{6} = \frac{1}{24}$. Let $\delta = 0.01$, then $\frac{8\delta_h^2 \ln 8/\delta}{\bar{h}_s} \approx 928$.

In addition, in the first conclusion of Theorem B.3.1 we consider weighted prediction values by h_i . Since with second-order approximation of the loss function, h_i influences how much a training sample contributes to the approximated loss by second-order Taylor expansion [5]. Thus, considering the weighted prediction values by h_i is meaningful.

Finally, the upper bound in Theorem B.3.1 requires a balanced split to be small. In other words, the data sizes in child nodes n_{s_1}, n_{s_2} shouldn't be significantly smaller than that in parent node n_s , so that the terms $\frac{n_s}{n_{s_1}\sqrt{n_{s_1}}}$ and $\frac{n_s}{n_{s_2}\sqrt{n_{s_2}}}$ can be bounded by a small value.

E New CUDA Framework of LightGBM

We implement a new CUDA version for LightGBM. Previous GPU versions of LightGBM only run histogram construction on GPUs. Our new implementation performs the whole training process

Table 6: Detailed time costs for different algorithms in different datasets (seconds).

	Algorithm	Higgs	Epsilon	Kitsune	Criteo	Bosch	Year	Yahoo LTR	LETOR
GPU total time	XGBoost	33.97 ±0.09	311.12 ±0.48	181.24 ±0.26	326.82 ±0.31	68.44 ±0.19	20.47 ±0.36	28.64 ±0.19	51.29 ±0.25
	CatBoost	61.10 ±3.98	105.00 ±0.00	80.20 ±1.72	187.80 ±1.17	22.12 ±0.30	33.96 ±2.04	59.22 ±0.37	N/A
	LightGBM+	29.05 ±0.22	87.12 ±0.39	77.43 ±0.50	102.33 ±1.61	21.41 ±0.44	24.33 ±0.30	30.79 ±0.20	41.79 ±0.42
	LightGBM+ 2-bit	24.78 ±0.31	39.04 ±0.31	38.26 ±0.12	61.04 ±0.27	12.57 ±0.29	18.19 ±0.07	23.09 ±0.47	33.60 ±0.29
	LightGBM+ 3-bit	24.45 ±0.36	39.25 ±0.31	38.63 ±0.52	59.93 ±0.37	12.60 ±0.39	18.24 ±0.18	24.93 ±0.42	33.87 ±0.38
	LightGBM+ 4-bit	24.53 ±0.26	39.82 ±0.15	40.00 ±0.24	59.49 ±0.26	12.55 ±0.27	18.34 ±0.20	25.65 ±0.38	34.11 ±0.12
	LightGBM+ 5-bit	24.55 ±0.14	41.30 ±0.10	40.83 ±0.46	60.24 ±0.37	12.08 ±0.24	18.41 ±0.15	25.50 ±0.40	34.36 ±0.07
	CPU total time	XGBoost	109.16 ±2.06	1282.97 ±12.53	281.72 ±4.84	565.52 ±1.54	130.92 ±0.45	28.85 ±0.47	103.87 ±0.46
CatBoost		1009.8 ±9.22	1283.4 ±3.32	1495.0 ±31.43	7702.2 ±55.16	998.4 ±30.36	95.8 ±1.17	588.2 ±4.83	865.4 ±9.13
LightGBM		83.27 ±0.41	519.89 ±1.91	332.12 ±4.17	524.61 ±9.32	59.94 ±0.08	12.67 ±0.11	75.44 ±0.37	103.09 ±1.05
LightGBM 2-bit		73.36 ±0.36	426.50 ±5.25	215.91 ±3.05	444.28 ±7.39	46.63 ±0.47	12.94 ±0.16	61.50 ±0.41	72.08 ±0.55
LightGBM 3-bit		69.64 ±0.50	459.39 ±2.83	207.96 ±2.45	440.68 ±38.97	47.35 ±0.30	12.79 ±0.22	61.07 ±0.41	74.35 ±0.29
LightGBM 4-bit		69.30 ±0.40	458.62 ±2.55	208.99 ±1.23	416.60 ±6.73	46.45 ±0.28	11.90 ±0.23	61.15 ±0.43	77.66 ±1.94
LightGBM 5-bit		69.86 ±0.93	457.68 ±2.81	211.53 ±4.20	423.80 ±19.23	47.52 ±1.54	11.79 ±0.09	61.76 ±0.45	77.92 ±0.50
GPU Hist. time	LightGBM+	11.26 ±0.03	46.96 ±0.18	54.77 ±0.37	70.97 ±1.33	16.57 ±0.41	9.61 ±0.03	11.59 ±0.09	17.75 ±0.24
	LightGBM+ 2-bit	4.84 ±0.03	12.11 ±0.07	16.41 ±0.13	21.74 ±0.10	8.52 ±0.29	4.08 ±0.02	8.23 ±0.25	10.20 ±0.07
	LightGBM+ 3-bit	4.74 ±0.07	12.25 ±0.08	16.07 ±0.15	21.14 ±0.07	8.49 ±0.32	4.11 ±0.02	8.54 ±0.27	10.29 ±0.09
	LightGBM+ 4-bit	4.74 ±0.04	12.51 ±0.03	16.45 ±0.12	21.02 ±0.10	8.44 ±0.29	4.15 ±0.02	8.66 ±0.25	10.52 ±0.04
	LightGBM+ 5-bit	4.70 ±0.04	13.54 ±0.02	16.78 ±0.09	21.31 ±0.15	7.93 ±0.25	4.24 ±0.03	8.60 ±0.31	10.78 ±0.05
CPU Hist. time	LightGBM	50.74 ±0.33	458.46 ±1.74	253.07 ±5.00	385.98 ±9.60	53.08 ±0.19	6.68 ±0.09	58.53 ±0.26	66.39 ±1.05
	LightGBM 2-bit	32.82 ±0.26	375.70 ±5.12	147.10 ±3.57	269.00 ±7.70	39.80 ±0.54	5.99 ±0.14	43.59 ±0.33	38.23 ±0.27
	LightGBM 3-bit	30.84 ±0.38	410.29 ±2.56	137.54 ±1.84	273.68 ±38.78	40.36 ±0.34	5.85 ±0.16	43.47 ±0.36	40.21 ±0.18
	LightGBM 4-bit	30.72 ±0.30	406.91 ±2.35	133.15 ±1.26	252.20 ±6.67	39.88 ±0.26	5.23 ±0.15	43.73 ±0.27	43.23 ±0.92
	LightGBM 5-bit	30.97 ±0.48	406.26 ±2.83	130.13 ±4.23	259.50 ±18.63	40.70 ±1.06	5.14 ±0.06	44.80 ±0.44	43.68 ±0.35

including boosting (calculation of gradients and Hessians) and tree learning on GPUs. We denote this new GPU version of LightGBM by LightGBM+ in our paper.

Table 7: Experiment Environments (CPU)

CPU	Intel(R) Xeon(R) Platinum 8370C
Cores	16 Physical CPU Cores
OS	Ubuntu 18.04
Memory	256 GB

Table 8: Experiment Environments (GPU)

CPU	Intel(R) Xeon(R) CPU E5-2690 v4
Cores	24 Physical CPU Cores
GPU	NVIDIA Tesla V100 PCIe 16GB
OS	Ubuntu 18.04
Memory	448 GB

Table 9: Hyperparameters of LightGBM

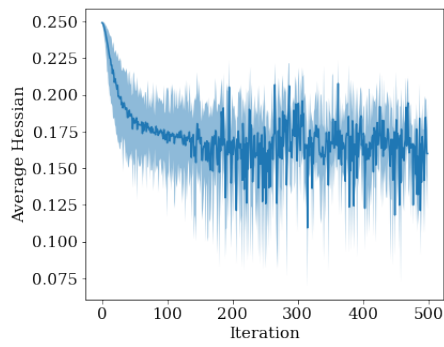
boosting_type	gbdt
learning_rate	0.1
min_child_weight	100
num_leaves	255
max_bin	255
num_iterations	500
num_threads	16
objective (binary)	binary
objective (regression)	regression
objective (ranking)	lambdarank
metric (binary)	auc
metric (regression)	rmse
metric (ranking)	ndcg@10

Table 10: Hyperparameters of XGBoost

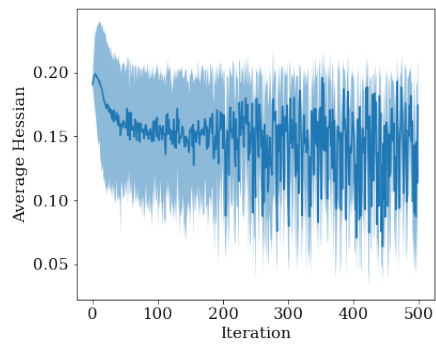
tree_method	hist/gpu_hist
eta	0.1
max_depth	0
max_leaves	255
num_round	500
min_child_weight	100
nthread	16
gamma	0
lambda	0
alpha	0
objective (binary)	binary:logistic
objective (regression)	reg:linear
objective (ranking)	rank:pairwise
metric (binary)	auc
metric (regression)	rmse
metric (ranking)	ndcg@10

Table 11: Hyperparameters of CatBoost

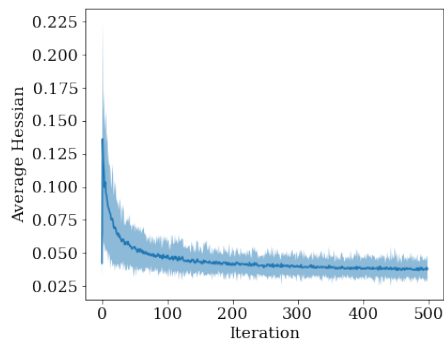
thread_count	16
border_count	255
iterations	500
learning_rate	0.1
grow_policy	Lossguide
boosting_type	Plain
max_leaves	255
depth	256
min_data_in_leaf	100
objective (binary)	Logloss
objective (regression)	RMSE
objective (ranking)	YetiRank
metric (binary)	AUC
metric (regression)	RMSE
metric (ranking)	NDCG:top=10;type=Exp
bootstrap_type	No
random_strength	0
rsm	1



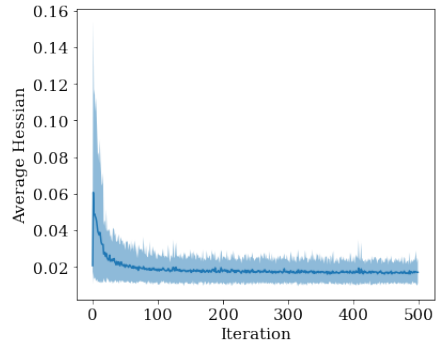
(a) Higgs



(b) Criteo



(c) Yahoo LTR



(d) LETOR

Figure 7: Average Hessian Values by Iteration with 3-Bit Gradients